In: Recent Studies in Materials Science ISBN 978-1-53615-270-8
Editor Patrick R. Lind

Chapter 2

CONVECTIVE EFFECTS AND TRAVELING WAVES IN TRANSPARENT OXIDE MATERIALS PROCESSED WITH THE FLOATING ZONE TECHNIQUE

Marcello Lappa*

Department of Mechanical and Aerospace Engineering,
University of Strathclyde, Glasgow, UK

ABSTRACT

Zone melting (or zone refining or floating zone process, FZ) is a group of similar methods, specifically conceived for the purification of crystals, in which thermally-driven flows of both gravitational and surface-tension natures are typically produced when the considered material is processed. Since the melt never comes into contact with anything but vacuum (or inert gases), there are no contaminants that the melt may incorporate. Even though compounds with higher purity and

* Email: Marcello.lappa@strath.ac.uk.

improved quality can be obtained with this technique, a typical drawback is represented by the defects potentially induced in the crystalline structure by the unavoidable convection emerging in the fluid phase. In the present chapter, special attention is paid to a specific category of materials known as transparent oxides. A range of conditions is explored, differing in the dominant effect (buoyancy or Marangoni flow), the thermal conditions (heating being provided along the radial or axial direction) and the relative direction of gravity and applied temperature gradient. The hallmark of the entire chapter is our commitment to identify situations in which "waves" are produced and provide a systematic classification of such convective instabilities together with a description of related features based on advanced numerical simulations.

1. INTRODUCTION

Relevant examples pertaining to the category of oxide transparent materials include (but are not limited to): yttrium aluminum ($Y_3Al_5O_{12}$), yttrium orthoaluminate ($YAlO_3$), spinel ($MgAl_2O_4$), sapphire (Al_2O_3), lithium tantalite ($LiTaO_3$) and gadolinium gallium garnet ($Gd_3Ga_5O_{12}$). These compounds constitute a basis for a variety of advanced industrial applications. Indeed, they are used for solid state lasers, and as magnetic bubble device substrates, insulating layers for semiconductors, or monolithic crystal filters. Moreover, the so-called transparent conductive oxides (TCOs), known for their unusual ability to possess transparent and conducting properties at the same time (Ohta and Hosono, 2004), are typically employed in flat panel displays (such as LCDs, i.e., liquid crystal displays), electroluminescent devices (e.g., organic light emitting diodes - OLEDs), solar cells and power saving opto-electrical circuitries (Stadler, 2012). Notably, the transparency property also applies to the related molten state, which is typically established at relatively high temperatures (e.g., the melting points of sapphire and yttrium aluminum are $\cong$ 2300 K and 2960 K, respectively).

The kinematic viscosity (ν) and thermal diffusivity (α) of all these melts have, in general, a comparable order of magnitude (with the former being slightly larger than the latter). This behavior formally puts these

substances in the general class of *high-Pr liquids*, where $Pr = \nu/\alpha$ is the so-called fluid Prandtl number. This parameter generally ranges in the interval $O(1) \leq Pr \leq O(10)$ and this might be regarded as a clear distinguishing mark with respect to other transparent insulating materials (e.g., SiO_2 glasses for which $Pr = O(10^3)$), organic substances such as molten hexatriacontane ($C_{36}H_{74}$, $Pr = 65$) and molten tetracosane ($C_{24}H_{50}$, $Pr = 49$) or opaque liquid metals and semiconductor (or superconductor) melts, for which $Pr<<1$.

From a purely industrial standpoint, transparent oxides are generally crystallized using different methods such as vapor-phase or liquid-phase epitaxial techniques or other processes which come under the heading of 'crystal-growth-from-the-melt' (relevant examples being represented by the Horizontal or vertical Bridgman technique, the Czochralski (CZ) method or the so-called Floating zone (FZ) process, Hurle, 1994; Lappa, 2009). A related key aspect is represented by the ability to transform the considered transparent compound, initially in a polycrystalline state, into a *single-crystal* while keeping the formation of impurities and defects *at minimum*. In such a context, many advantages are provided by the *FZ process* given its (known) matchless ability to reduce melt contamination potentially induced by the interaction of the high-temperature melt with external walls or parts.

The FZ process starts from a cylindrical rod of the considered polycrystalline material to be melted in a controlled environment (an inert gas or vacuum) via the application of localized heating to its surface. Such heating is generally provided in order to preserve the initial symmetry of the specimen, i.e., by means of a coaxial ring heater or an optical furnace relying on curved (circular) mirrors. The rod does not hold a stationary position with respect to the heating device. Rather relative motion is established between the material and the limited region subjected to localized heating. In this way, an ongoing process is maintained where a new portion of the polycrystalline bar undergoes melting while the liquid re-solidifies as a single crystal (the 'seed') at the other side of the liquid zone. This means that, at any instant, the entire amount of molten material is suspended (in the form of a 'liquid bridge') between the initially impure

solid and the seed (which illustrates why these crystallization processes come under the common heading of "Floating Zone" approach).

The intrinsic advantages become readily evident if one considers that the liquid is never in contact with a container or a crucible, which may dissolve thereby altering its composition. As a result, crystals with higher purity can be produced (see, e.g., Benz, 1990). These advantages have made these methods increasingly popular for the production of a wide range of materials, including metals, semiconductors (Cröll et al., 1998), high-temperature superconductors, new magnetic materials and oxides (Saurat and Revcolevsch, 1971; Shindo et al., 1979; Shindo, 1980; Balbashov and Egorov, 1981; Kimura and Kitamura, 1992; Revcolevschi and Jegoudez, 1997; Moest et al., 1998). In particular, transparent oxides typically processed with the FZ are substances such as β-Ga_2O_3 (Villora et al., 2004) or TiO_2 (Higuchi and Kodaira, 1992; Watauchi et al., 2012), and more complex compounds such as $CuGeO_3$ (Revcolevschi and Jegoudez, 1997) and $Y_3Fe_5O_{12}$ (Balbashov et al., 1975; Shindo et al., 1979; Balbashov and Egorov, 1981). The interested reader is referred to the works by Dabkowska and Gaulin (2003) and Dabkowska and Dabkowski (2010) for an exhaustive review of materials processed with the FZ technique.

Here, we concentrate on a specific aspect, that is, the fluid convection occurring in the molten zone (the aforementioned "liquid bridge"), given its known ability to induce undesired (often unavoidable) compositional and structural defects in the final crystals (Muller, 1988).

Fluid motion obviously arises as a consequence of the significant thermal gradients being present in the melt as a result of the temperature difference between relatively cold regions (where the material is solid) and those where heating is applied.

Remarkably, these gradients can support two concurrent mechanisms driving fluid motion, the first being obviously represented by the well-known dependence of the density of liquids on temperature (which, by enabling buoyancy effects, can lead to convection of thermogravitational nature). The second relates directly to the existence of a free surface in the considered process, namely the interface that separates the melt region from the external environment (be it an inert gas or vacuum). The stable

existence of this surface is allowed by surface tension (σ) that, by counteracting gravity, prevents the liquid from being pulled down. As the surface tension depends on temperature (the higher the temperature, the smaller σ), any temperature gradient established along the interface is directly turned into a gradient of surface tension forcing the fluid to move from warmer surface regions towards colder ones. The related mechanism is generally known as thermocapillary (or Marangoni) convection.

Even though their relative strength can vary depending essentially on the considered fluid and the effective extension of the liquid zone, in typical industrial applications these two forms of convection are always simultaneously present (Lappa, 2009, 2012). Their relative importance or weight can also have a remarkable impact on the so-called *hierarchy of bifurcations*, i.e., the specific path followed by these systems when the temperature difference (ΔT) is increased. A rise in the ΔT typically results in the flow undergoing *various symmetry breaking phenomena* and in *the onset of time-dependence*. The precise sequence of events, however, does depend on various parameters and on the dominant driving force.

The present chapter is entirely devoted to a focused review of these modes of convection in physical domains with cylindrical symmetry (assumed to mimic the real FZ process), together with a critical analysis of very recent findings.

Given the impressive amount of literature existing on these subjects, we limit ourselves to discussing fluids with $Pr \geq O(1)$ representative of transparent oxides, the reader being referred to Lappa (2007) for an analogous treatment concerning liquid metals and semiconductor melts.

Emphasis is also given to aspects relating to the "pattern formation", particularly for the circumstances in which thermocapillary and thermogravitational convection, in disjoint or combined form, can produce undesired *waves traveling* in the considered fluid system. With the descend of scale, localized defects produced by such waves in the material start to be dominating with respect to other types of defects induced by large-scale flow; complex interplay of these together contributes to significant manufacturing challenges (Hurle, 1994).

In order to place all these phenomena in a proper theoretical context, we provide relevant details about the overarching fluid-dynamic equations, typical mathematical models used for the FZ technique, the related boundary conditions and underlying assumptions. Along the same lines, the discussion is supported by a variety of numerical results to show the considered dynamics with a level of detail that is hardly achievable by experimental analysis and/or direct flow visualization.

2. MATHEMATICAL MODELS

2.1. Governing Equations

Referring velocity and temperature to the scales α/L and ΔT, respectively and scaling all distances on L, where L is a characteristic length for the considered problem and α is the liquid thermal diffusivity, the overarching balance equations for mass, momentum and energy transport in the molten material can be cast in condensed form as :

$$\underline{\nabla} \cdot \underline{V} = 0 \tag{1}$$

$$\frac{\partial \underline{V}}{\partial t} = -\underline{\nabla} p - \underline{\nabla} \cdot \left[\underline{V}\,\underline{V}\right] + \mathrm{Pr}\,\nabla^2 \underline{V} - \mathrm{Pr}\,Ra\;T\;\underline{i}_g \tag{2}$$

$$\frac{\partial T}{\partial t} + \underline{\nabla} \cdot \left[\underline{V} T\right] = \nabla^2 T \tag{3}$$

where $\underline{V}$, T and p are the nondimensional velocity, temperature and pressure, respectively and $\underline{i}_g$ is the unit vector along the direction of gravity. The parameter $Ra = \dfrac{g\beta_T \Delta T L^3}{\nu\alpha}$, known as the Rayleigh number, essentially results from the application of the so-called Boussinesq approximation (Lappa, 2009) to the term accounting for the buoyancy

force in the momentum equation (where a linear relationship is assumed between density and temperature via the thermal expansion coefficient β_T). The Rayleigh number formally measures the relative importance of buoyancy and viscous forces.

Closure of the problem from a mathematical point of view, however, also requires that proper boundary conditions are used to complement eqs. (1)-(3). This means that a more complete mathematical framework must be defined, i.e., an abstraction of physical reality sufficiently simple to allow the treatment of the considered problem with a limited number of parameters and, at the same time, able to retain the physical mechanisms which are thought to be significant or of specific interest. Along these lines, the next section is entirely devoted to a presentation of the mathematical models which have enjoyed widespread use over recent years for the FZ process.

2.2. Geometrical Models of the FZ Technique

As explained above, the approach is to consider surrogates of the FZ that incorporate the presumed influential (behavior-determining) process(es). Irrespective of the approach used to define them, these configurations are approximate, i.e., a series of choices have to be made in their formulation, which may be dictated by convenience or simplicity or by the need to concentrate on some specific aspects.

In general, these distinct models can be delineated by retaining or disregarding the possible symmetries of the real FZ along different spatial directions. Prior to embarking in the description of them, we wish to remark that the existence of these symmetries implies the possibility of symmetry breaking (a very important concept in fluid-dynamics, given its deep connections with the notion of flow instability and bifurcation, which will be treated later in this chapter).

The simplest approximation for the FZ process is represented by a liquid zone with cylindrical interface held between two disks at different temperature, ideally assumed to model the heat and mass transfer processes

occurring between the equatorial plane of a real floating zone (where heating is applied) and one of the two horizontal solid surfaces (where liquefaction or solidification takes place depending on the considered portion of the rod). As this model accounts only for half size of the effective liquid region, it is generally known as the 'half zone' (Figure 1a). As the main direction along which the temperature difference is applied is *axial*, for simplicity, the free interface is generally approximated as an adiabatic boundary.

This assumption, however, must necessarily be removed when the more sophisticated 'full zone' is considered (Figure 1b). With this alternate configuration, heat is injected into the liquid through the free surface (along the radial direction, as it occurs in reality). The two ends of the domain perpendicular to the axial direction are therefore set at the same temperature (ideally mimicking the melting/solidification point of the considered material).

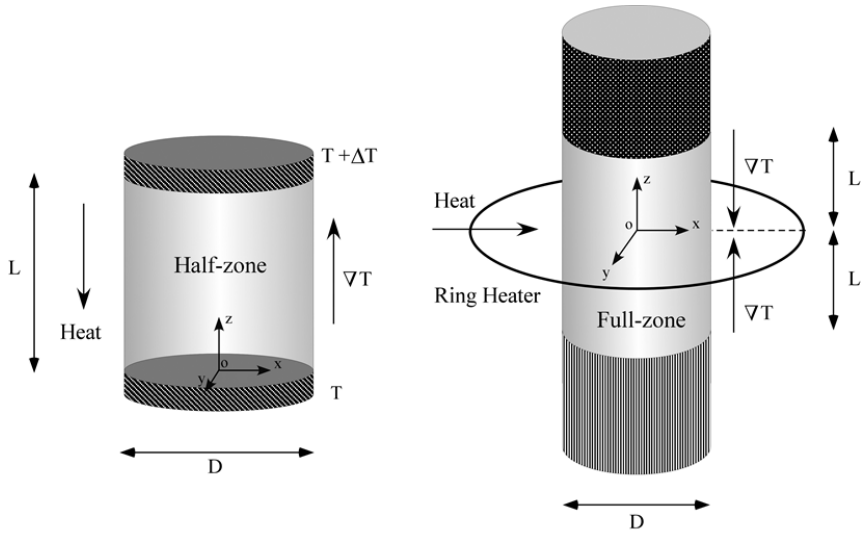

Figure 1. Main models of the FZ process and related boundary conditions: a) the Half Zone, b) the Full Zone.

The aspects, for which the two models can be distinguished, however, are not limited to the direction along which heat is injected into the liquid. As the reader may expect (given the introductory arguments given at the beginning of this section), a substantial difference can be found in the *symmetries* that can be broken by the flow. With the half zone, obviously, any processes that depend on the rupture of symmetry with respect to the vertical direction are excluded.

This degree of freedom, however, is present in the full zone, where the fluid *can cross the equatorial plane*. While a single toroidal roll is established in the half zone as a result of thermally driven convective effects, the full zone typically features two opposite toroidal rolls in the two regions which extend from the equatorial plane towards the solid supports. The ideal mirror symmetry of these two counter-rotating circulation systems with respect to the equatorial plane can be lost, leading to overlying rolls displaying different axial extension or even coalescing.

As a common feature, obviously both models allow symmetry breaking with respect to the azimuthal direction, which explains why the half zone has enjoyed so much attention over the last years as a relevant configuration to investigate the onset and propagation of the aforementioned waves (which in such systems travel essentially in the *azimuthal direction*).

From a purely mathematical standpoint, assuming the two supporting disks to be located at z = 0 and z = 1, respectively (reference length L equal to the distance separating the disks), for the half zone, the relevant thermal boundary conditions can be cast in condensed form as:

$$T(z = 0, r, \varphi, t) = T_{Bottom} \quad 0 \le r \le 1/A_H \; ; \; 0 \le \varphi \le 2\pi \tag{4a}$$

$$T(z = 1, r, \varphi, t) = T_{Top} \quad 0 \le r \le 1/A_H \; ; \; 0 \le \varphi \le 2\pi \tag{4b}$$

where $A_H = L/D$ is the aspect ratio, φ is the azimuthal angle and $T_{Bottom} = 0$ and $T_{Top} = 1$ or $T_{Bottom} = 1$ and $T_{Top} = 0$ according to whether the liquid

bridge is *heated from above or from below*, respectively. At the free interface the condition of adiabaticity simply results in:

$$\frac{\partial T}{\partial r}(z, r = 1/2A_H, \varphi, t) = 0 \tag{5}$$

For the full zone, as explained before, the two ends must be set at the same temperature. Assuming as reference length L the axial distance between the equatorial plane containing the ring heater and one of the supporting disks (see Figure 1b), related thermal conditions read:

$$T(z = -1, r, \varphi, t) = 0 \quad 0 \le r \le 1/A_F \; ; \; 0 \le \varphi \le 2\pi \tag{6a}$$

$$T(z = 1, r, \varphi, t) = 0 \quad 0 \le r \le 1/A_F ; \; 0 \le \varphi \le 2\pi \tag{6b}$$

where $A_F = 2L/D = 2A_H$. In this case, a slightly more complex treatment is required for the interface as the condition of no heat flux (eq. (5)) must be replaced by an adequate mathematical expression accounting for the radiative heat transfer from the heating system to the liquid surface. Many models have been proposed in literature to simulate surface heating due to a ring heater (see, e.g., Otani et al., 1988; Rivas and Vazquez-Espi, 2001). Following Lappa (2016), the radiative flux generated by a coaxial ring heater with negligible thickness located at a fixed distance h from the free surface can be modeled in a relatively straightforward way starting from the radiative contribution brought to the overall flux by each infinitesimal portion of the ring. Indeed, taking into account the details shown in Figure 2, this contribution can formally be expressed as:

$$j(z) = \left(\frac{1}{L\lambda}\right)\frac{1}{4\pi}\frac{\xi\overline{Q}}{\delta^2}\cos(\theta) \tag{7a}$$

where $\overline{Q}$ is the overall power consumed by the ring heater, δ represents the distance between two generic points lying respectively on the ring heater (C)

and on the interface (P) and θ denotes the angle comprised between the direction PC and the unit vector $\underline{\hat{n}}$ perpendicular to the free surface in P.

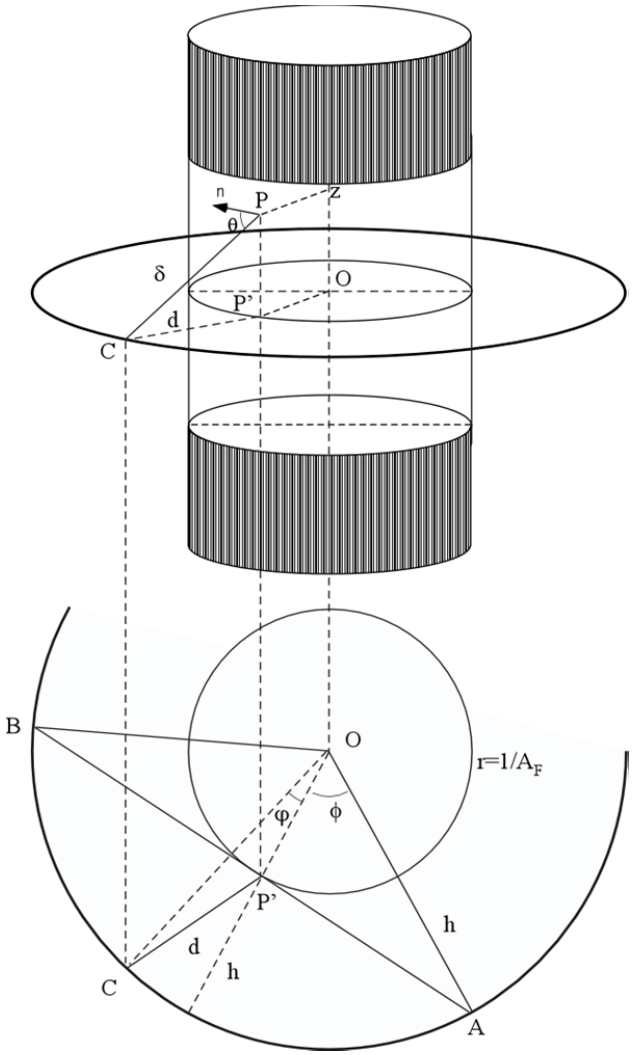

Figure 2. Sketch of the floating zone and related ring heater.

Integration of the infinitesimal contribution along the entire circumferential extension formally gives the effective (local) flux as:

$$J(z) = \frac{1}{4\pi}\left(\frac{\xi \overline{Q}}{L\lambda}\right) \int_{-\tilde{\phi}}^{\tilde{\phi}} \frac{\cos(\theta)}{\delta^2}\, d\varphi \tag{7b}$$

where:

$$\delta^2 = \frac{1}{A_F^2}\left[(1+hA_F)^2 + 1 - 2(1+hA_F)\cos\varphi + z^2 A_F^2\right] \tag{8a}$$

$$\cos(\theta) = \frac{(1+hA_F)\cos\varphi - 1}{\sqrt{\left[(1+hA_F)^2 + 1 - 2(1+hA_F)\cos\varphi + z^2 A_F^2\right]}} \tag{8b}$$

$$\tilde{\phi} = \cos^{-1}\frac{1}{(1+hA_F)} \tag{8c}$$

and ξ is the free-surface emissivity. Therefore, eq. (5) must be replaced by

$$\frac{\partial T}{\partial r}(z, r = 1/A_F, \varphi, t) = J(z) \tag{9}$$

Yet from a mathematical point of view, problem 'closure' also requires relevant kinematic conditions along the boundary. For solid surfaces these reduce to the trivial condition of no-velocity (no-slip), i.e., $\underline{V} = 0$.

On the free surface, however, the velocity cannot be imposed directly. Indeed, it must satisfy a dynamic balance between the viscous shear stress in the liquid and the gradient of surface tension. In non-dimensional form such a balance can be cast in compact form as:

$$\left[2\left(\underline{\nabla V}\right)^s\right]\cdot\hat{\underline{n}} = -Ma\left(\underline{\underline{I}} - \hat{\underline{n}}\hat{\underline{n}}\right)\cdot\underline{\nabla T} \tag{10}$$

where $\left(\underline{\underline{\nabla V}}\right)_o^s = \dfrac{\underline{\underline{\nabla V}} + \underline{\underline{\nabla V}}^T}{2}$ and *Ma* is the so-called Marangoni number, $Ma = \mathrm{Re}\,\mathrm{Pr} = \dfrac{\sigma_T \Delta T L}{\mu\alpha}$ (μ being the fluid dynamic viscosity and σ_T the derivative of surface tension with respect to temperature). This number plays for thermocapillary flows the same role that the Rayleigh number has for thermogravitational flows.

Accordingly, a relevant parameter used to characterize the relative importance of surface-tension driven and buoyancy effects (the so-called dynamic Bond number) can be introduced as:

$$B_d = \frac{Ra}{Ma} \tag{11}$$

There are many numerical techniques that can be used to solve directly all these equations (and related boundary conditions) or get useful information from simplified versions of them (e.g., via linear stability analysis). Clarifying the advantages or bottlenecks associated with each different approach is not as straightforward as one would imagine. In this section we will merely touch on this subject, which would otherwise occupy the entire chapter (the reader specifically interested in these aspects may consult the extensive information reported in a companion chapter of this book, Lappa and Ferialdi, 2019).

In particular, we limit ourselves to pointing out that the so-called category of *projection method*s has already proven to be a relevant choice for the simulation of the fluid-dynamic instabilities in floating zones, as witnessed by the many research articles appearing in the literature (Yasuhiro et al., 1997, 1999; Lappa et al., 2000 and 2001; Melnikov et al., 2005; Shevtsova et al., 2001, 2003, 2011; Lappa, 2016). Remarkably, with gained confidence in the validity of these methods, research on these subjects is still progressing and it can still be considered nowadays as a very active line of inquiry.

All the (representative) numerical results described in this chapter have been obtained in the framework of such techniques.

Given the spirit of the present book, conceived to provide readers with applicative aspects and insights into recent findings, such examples are essentially used to support the discussion and explain the 'physics' of the considered phenomena (Sects. 3 and 4). For the above reasons, details about the used meshes, numerical schemes and accuracy are glossed over, the reader being referred directly to the articles cited in the text for additional details.

In particular, most of results are presented for Pr > 10 given the widespread use of such liquids in the literature as surrogate models of oxide melts.

3. THE LIQUID BRIDGE

This section is entirely devoted to the popular classical liquid bridge or half zone (hereafter these two terms will be used as synonyms), given its success over the years as an archetypal model for the study of the fundamental properties of Marangoni flows and related hierarchy of bifurcations. As illustrated in Sect. 2.2, this configuration offers several advantages to investigators, especially, the possibility to set a precise temperature difference 'a priori' and assess the system response for increasing values of it, which explains why this model has attracted the attention of research groups with various interests and motivations, leading over the years to the emergence of a common theoretical framework that is generally referred to as the *liquid-bridge problem*. In the following we present a brief account of the historical perspective that led to this framework and its diverse reverberations in the science of fluids and materials.

3.1. Pure Thermocapillary Flow

The mathematical aspects of this problem have been defined in the previous section (see, in particular, Figure 1a and eqs. (4)-(5)). The liquid

bridge or half zone can essentially be seen as a differentially heated portion of liquid delimited by a cylindrical free liquid-gas interface. The thermocapillary (Marangoni) flow established in the liquid is initially steady and laminar and reflects the symmetry properties of the hosting domain (i.e., it is axisymmetric). However, when the temperature difference is sufficiently increased (the Marangoni number exceeds a given threshold), the flow becomes three-dimensional. For the case of oxide melts (in particular) and for all high-Pr liquids (in general), the symmetry breaking process is intimately associated with the onset of time-dependence, i.e., the flow becomes 3D and oscillatory at the same time.

This field has reached a certain level of maturity. Experiments conducted in space (e.g., on-board sounding rockets or on the space shuttle, see, e.g., Schwabe et al., 1982; Schwabe and Scharmann, 1984; Monti, 1987; Monti et al., 1995; Chun and Siekmann, 1995; Monti et al., 1998; Schwabe, 2002 and 2005, etc.) have been instrumental in clarifying that this type of instability does not depend on gravity and it should therefore be regarded as an intrinsic 'property' of Marangoni flow (Figure 3).

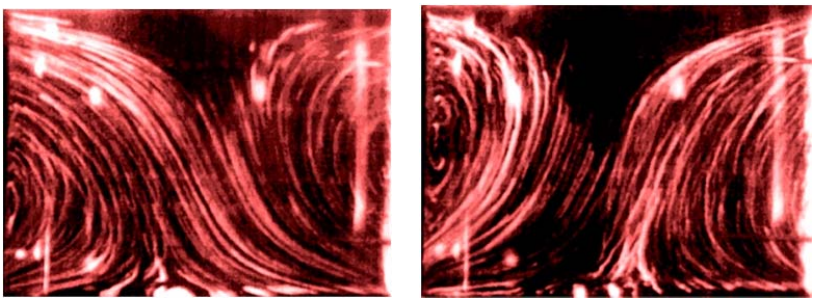

Figure 3. Typical structure of oscillatory Marangoni convection in the meridian plane of a half zone (the motion of tracers is used to visualize the flow; tracers are illuminated by the light generated by a laser diode forming a light sheet perpendicular to the main optical path of a CCD camera; the two snapshots refer to experiments carried out during the Spacelab D2 mission; courtesy of the Microgravity Advanced Research and Support Center).

From an historical standpoint, interestingly, the analysis of this specific problem has progressed through relevant synergy between experimental activities and mathematical arguments based on the application of stability analyses (Neitzel et al., 1992; Kuhlmann and Rath, 1993a; Wanschura et al., 1995; Kuhlmann et al., 1995; Chen et al., 1997). As evident after comparative readings of these studies, starting from considerations based on the axial symmetry of the liquid bridge, it has been shown that 1) the oscillatory disturbances always emerge as *a couple of waves traveling in opposite directions* (namely, a pair of *clockwise and anticlockwise oriented trains of disturbances*) and 2) the specific patterning behavior displayed by the unstable flow in the supercritical regime essentially follows from the *interplay of such waves*.

As originally illustrated by Kuhlmann and Rath (1993b), by modeling each wave as a disturbance with expression $F_{\pm} = B_{\pm}(r,z)\exp\left\{i\left[\pm m\varphi - \omega t + G(r,z)\right]\right\}$ (where B(r,z) is the wave amplitude, G(r,z) is the phase, m is the wavenumber and $\omega = 2\pi f$ is the angular frequency), and by denoting with η the wave amplitude ratio, the functions expressing wave superposition can be cast in condensed form as:

$$F = 2B(r,z)\cos(m\varphi)\cos(\omega t - G(r,z)) \quad (\eta = 1) \tag{12}$$

$$F \cong B(r,z)\ \mathrm{a}(m\varphi)\cos\left[\mathrm{b}(m\varphi,G) - \omega t\right] \quad (0 < \eta < 1) \tag{13}$$

$$\text{with } \mathrm{a}(m\varphi) = \left[\ (1+\eta)^2\cos^2(m\varphi-\varphi_o) + (1-\eta)^2\sin^2(m\varphi-\varphi_o)\ \right]^{1/2} \tag{14a}$$

$$\text{and } \mathrm{b}(m\varphi,G) = \tan^{-1}\left[\frac{1-\eta}{1+\eta}\tan(m\varphi-\varphi_o)\right] + G(r,z) \tag{14b}$$

Assembled in this way, eqs. (12) and (13) have a straightforward physical interpretation. As the reader will easily realize, they differ essentially for the location of the group of variables (mφ) at the right hand-side. While in eq. (13) this group is an integral part of the oscillatory term

$\cos\left[\mathrm{b}(m\varphi, G) - \omega t\right]$, in eq. (12) the dependences on space (φ) and time (t) manifest in disjoint form, namely, $\cos(m\varphi)$ and $\cos(\omega t - G(r,z))$. This apparently innocuous observation has significant consequences on the spatio-temporal dynamics. While in the first case, the maxima and minima of the function *F* at given azimuthal positions can periodically swap their position as soon as cos(*ω*t-G(r,z)) changes its sign, in the second case the phase of the oscillations depends continuously on φ (which indicates that maxima and minima can continuously travel along the azimuthal direction).

Put differently, according to such arguments, while the superposition of two counter-propagating waves with the same amplitude should simply result in a pattern where the disturbance *nodes occupy fixed positions in space* (a waveform with disturbances growing and shrinking in time at fixed locations in the azimuthal direction), different amplitudes should lead to a pattern whose hallmark is the *visible rotation of features about the symmetry axis*. Using typical nomenclature introduced in the relevant literature, these two possible spatiotemporal modes of convection (waveforms) can also be simply referred to as: the *standing wave* (featured by disturbance nodes pulsating at fixed azimuthal positions, also known as *pulsating pattern*) and a *rotating pattern* (with disturbances traveling circumferentially, for simplicity generally called *traveling wave*).

Continuing with historical developments, it is worth mentioning that the existence of these states has been confirmed by experiments conducted both in space and on the ground (see, e.g., Velten et al., 1991; Frank and Schwabe, 1997; Savino et al., 2001; Schwabe, 2002). In facts, these spatio-temporal behaviors have been directly observed through visualization of tracer particles dispersed in the fluid (through one of the supporting disks made of a material transparent to visible light), or they have indirectly been detected *through analysis of the temperature signals provided by thermocouples at fixed positions* evenly distributed along the circumferential direction.

Following up on this point, the related rationale can directly be gathered from eqs. (12) and (13). As predicted by the first of these two

equations, when the flow is a standing wave, all the signals measured by thermocouples located at the same axial and radial coordinates (with different azimuthal positions) must be *in phase or in phase opposition* (put simply, only two values of phase shift are possible, namely $\Delta G = 0$ or $\Delta G = \pi$). For the traveling wave, the set of allowed phase shifts is *continuous* with ΔG (as illustrated, e.g., by Lappa et al., 2001, the phase shift is linearly proportional to the angular distance separating the thermocouples, provided such a distance $\Delta\varphi$ is shorter than π/m).

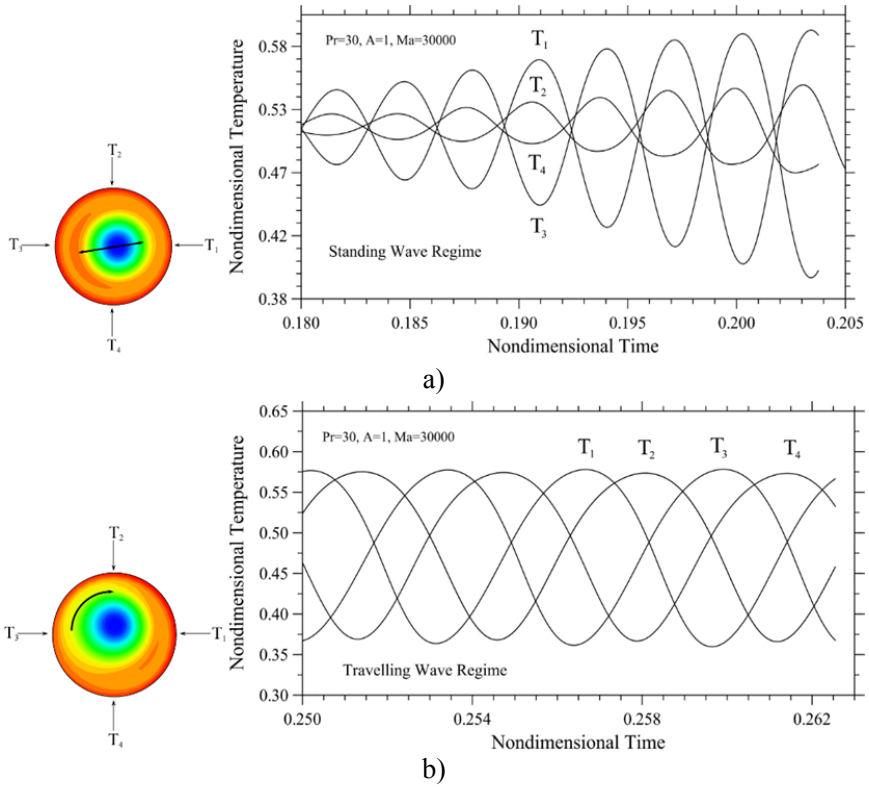

Figure 4. Snapshot of temperature distribution in a section perpendicular to the liquid bridge axis (left view, red and blue colors correspond to regions of relatively hot and cold fluid, respectively) and related temperature signals (right view) provided by four numerical probes periodically positioned at different azimuthal stations along the entire circumferential extension ($A_H = 1$, $Pr = 30$, $Ma = 3x10^4$, $m = 1$): a) pulsating temperature pattern (standing wave), b) rotating temperature pattern (traveling wave).

In parallel to experiments, numerical simulations have also been instrumental in leading to an exhaustive characterization of these dynamics (see, e.g., Lappa, 1995; Yasuhiro et al., 1997, 1999; Tang et al., 1997; Bazzi et al., 1999; Zeng et al. 1999a,b; 2001b; Leypoldt et al., 2000; Melnikov et al., 2005; Shevtsova et al., 2001, 2003, 2011).

As an example, Figure 4 shows the case for which four thermocouples equally spaced along 360° are used to compare the temperature signals relating to a flow with azimuthal wavenumber m = 1.

It can be seen that in this case the pattern in a cross section perpendicular to the liquid bridge is characterized by the presence of an inner region of colder fluid (this being a typical signature of Marangoni flow in liquid bridges). For m = 1 this region has approximately a circular shape and takes an eccentric position with respect to the point corresponding to the axis of the liquid bridge.

When the flow behaves as a standing wave, such a cold region undergoes back and forth motion along a fixed direction (highlighted by the double black arrow in Figure 4a). As a result the signals measured by the thermocouples display the behavior shown in the underlying plot, i.e., their peaks and valleys align at fixed time stations (in the figure, the valley measured by T_3 and the peak measured by T_1 correspond to the left-most displacement of the internal cold region and vice versa).

For the traveling wave, as evident in Figure 4b, all the peaks and valleys are aligned along the horizontal direction and the temporal distance between two consecutive peaks or valleys is always the same. This indicates that there is no preferred position for the disturbance nodes along the circumferential extension of the liquid bridge and that the center of the aforementioned inner eccentric region simply describes in space a circle, i.e., it travels continuously along the azimuthal direction (in this case the valley measured by each thermocouple corresponds to the instant at which the distance between the considered probe and the inner eccentric region attains a minimum).

Besides temporal features, some differences can also be seen in the spatial morphology taken by the isosurfaces of the azimuthal velocity component at a given instant. As shown in Figure 5a yet for the mode m =

1, for the standing wave, the isosurfaces located in proximity to the free surface look like two opposite “pillows” (corresponding to positive and negative values of the azimuthal velocity, respectively), each confined to one of the two halves of the liquid bridge that would be obtained by cutting it with a plane perpendicular to its bases and containing its axis. As evident in Figure 5b, however, such a ‘mental divisibility’ is no longer applicable to the traveling wave; when the disturbances rotate, no plane can be identified satisfying such a property regardless of the considered instant. The two pillows are inclined with respect to the axial direction and oriented in such a way that regions of the surface exist where the velocity component close to the bottom disk is positive while it has the opposite sign close to the top (and vice versa).

Additional examples about the typical behavior of standing and traveling waves have been reported in Figures 6 and 7 for a different value of the azimuthal wavenumber.

As the reader will easily realize by inspecting these figures, a general description in terms of eqs. (12)-(14) would still be possible provided m = 1 is replaced with m = 2.

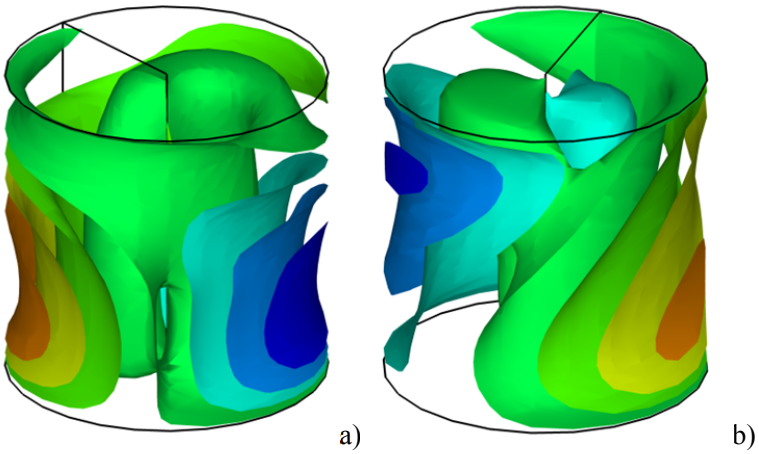

Figure 5. Isosurfaces of azimuthal velocity component for the same conditions shown in Figure 4a and 4b, respectively (red and blue colors correspond to regions of positive and negative azimuthal velocity, respectively).

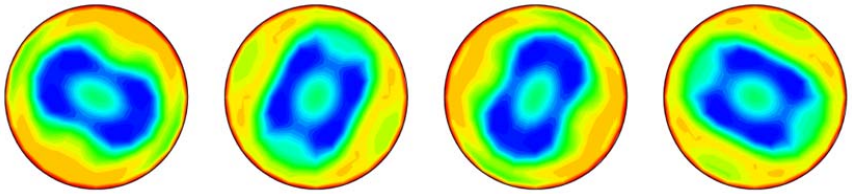

Figure 6. Snapshot of temperature distribution in a section perpendicular to the liquid bridge axis ($A_H = 0.4$, Pr = 30, Ma = $3.6x10^4$, m = 2, Standing Wave, red and blue colors correspond to regions of relatively hot and cold fluid, respectively).

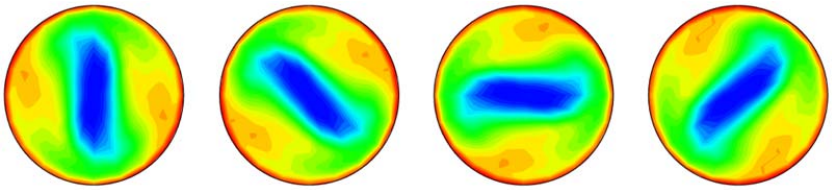

Figure 7. Snapshot of temperature distribution in a section perpendicular to the liquid bridge axis ($A_H = 0.4$, Pr = 30, Ma = $3.6x10^4$, m = 2, Traveling Wave, red and blue colors correspond to regions of relatively hot and cold fluid, respectively).

Having completed a characterization of these dynamics from a mathematical point of view, a further understanding of the instability is now gained by considering the *mechanism* by which the two counteracting hydrothermal waves postulated for the derivation of eqs (12)-(14) can be *initiated* in the physical reality (and lead to the subsequent stages of evolution with pulsating or rotating flow features, such as those shown in Figure 4-5 and Figures 6-7 for m = 1 and m = 2, respectively).

In particular, following Chun (1980), we introduce a relatively simple physical interpretation for such mechanisms by considering a localized disturbance on the free surface of the liquid bridge. As originally argued by this author, a temperature disturbance emerging spontaneously on the surface can immediately induce a convective disturbance in the velocity field given it ability to produce locally a temperature gradient in the circumferential direction and therefore a gradient of the surface tension. The modification of the velocity field with respect to that existing prior to the spontaneous emergence of the temperature disturbance, in turn, can alter the temperature distribution. This process can enable and sustain a

feedback mechanism by which the original disturbance is amplified or mitigated depending on the considered conditions.

This is shown in detail in Figure 8a-8d. An initial hot disturbance can generate two opposite surface currents moving far away from it. For continuity, liquid present in the bulk tends to move along a radial direction from the internal region (which, as explained before, is generally colder than the surface) towards the position of the initially hot disturbance. As a result, the radial current of cold flow can turn the initial hot disturbance into a cold perturbation. Once a cold spot has been produced, it can induce a modification of the axial component of the surface velocity (Figure 8e). Indeed, the strength of surface flow axially directed from the hot disk to the cold one will increase locally (in a position located upstream with respect to the disturbance). This final effect can overheat the initial cold disturbances, thereby leading the system to recover its initial condition with the hot spot located in that position (Zeng et al., 2004).

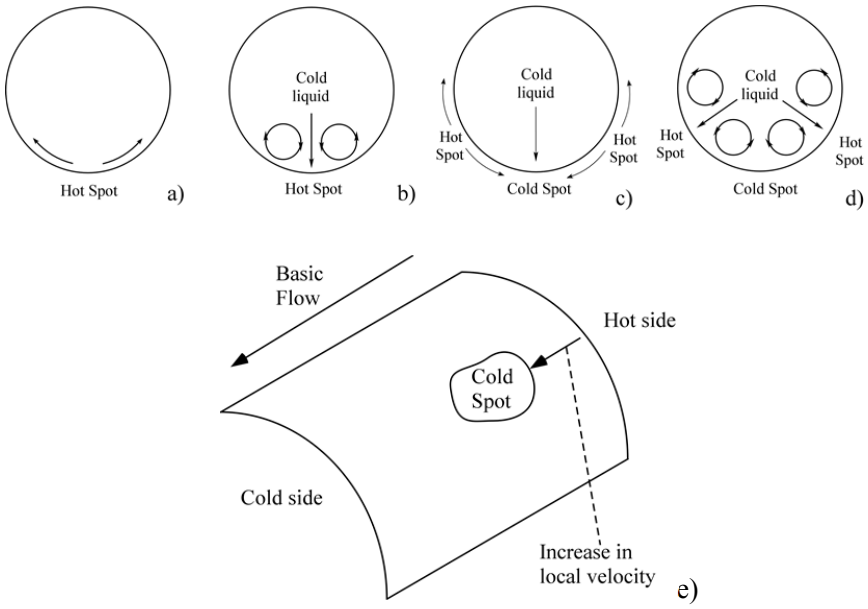

Figure 8. Amplification mechanism (sketch) leading to the emergence of counter-propagating hydrothermal waves (Marangoni convection in liquid bridges).

These dynamics are not possible for low-Pr because as in the case of liquid metals or semiconductor melts, owing to the relatively high thermal diffusivity of the liquid, any temperature disturbance would quickly be damped, thereby preventing it from coupling with convective effects as illustrated in Figure 8. By contrast, for Pr≥O(1) the mechanism summarized in Figure 8a-8e by which the hot and cold disturbances replace periodically can be turned into an everlasting phenomenon. This figure also makes evident how a disturbance initially emerging at a given azimuthal position can indirectly induce disturbances at other positions, thereby leading to the emergence of a spatially extended *pattern*, i.e., a given number of circulations in the generic section perpendicular to the liquid bridge axis (a total of 2*m* convective cells, *m* cells with the fluid circulating in the clockwise direction and *m* cells oriented in the opposite direction).

Interestingly, some useful considerations on the relationship between the azimuthal wavenumber *m* and the aspect ratio of the liquid bridge can be introduced on the basis of relatively simple geometrical arguments. As illustrated experimentally by Preisser et al. (1983), the radial penetration depth of convection in the bulk of the liquid is approximately given by the extension along z of the toroidal convection roll (L_V); as schematically shown in Figure 8d, the azimuthal extension of the convective cells induced by the flow instability in the cross sections perpendicular to the liquid zone axis is also approximately equal to the radial extension (L_V) of the toroidal vortex; this leads to the conclusion that the 2*m* circulations cells cover a circumference $2mL_V$. By expressing the circumference of the toroidal vortex as πD_V where D_V is its diameter, these arguments finally give rise to the following analytical relationship:

$$mA_V = \frac{\pi}{2} \rightarrow mA_H \cong 1 \tag{15}$$

where $A_V = L_V/D_V$ and $A_H = L/D$ are the aspect ratio of the Marangoni toroidal vortex and of the half zone, respectively. The agreement between

this formula and available results is witnessed by both existing experiments (Figure 9) and numerical results (see, e.g., Figure 10)

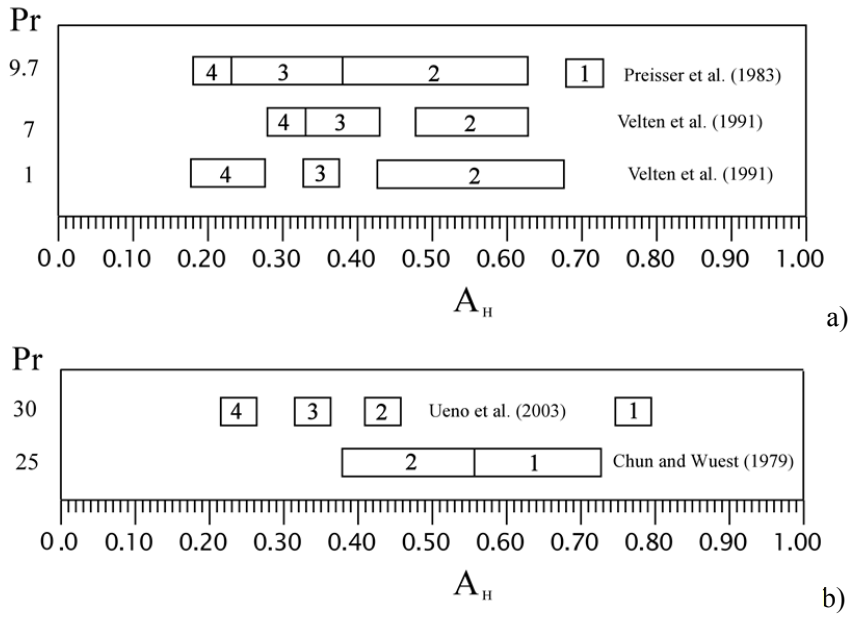

Figure 9. Critical azimuthal wavenumber versus the aspect ratio A_H for different values of the Prandtl number Pr≥1 as determined in landmark experiments (with liquid bridges heated from above in normal gravity conditions): a) Pr < 10, b) Pr > 10.

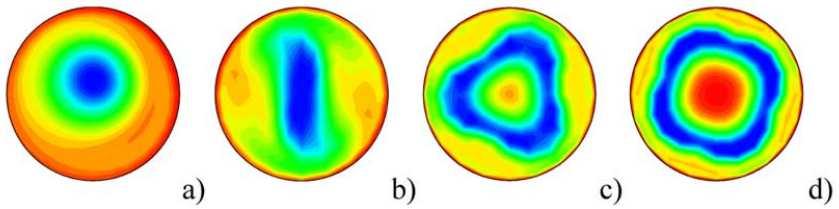

Figure 10. Snapshots of temperature distribution in a section perpendicular to the liquid bridge axis for decreasing values of the aspect ratio (Pr = 30, red and blue colors correspond to regions of relatively hot and cold fluid, respectively): a) $A_H = 1$, Ma = $3x10^4$, m = 1; b) $A_H = 0.4$, Ma = $3.6x10^4$, m = 2; c) $A_H = 0.25$, Ma = $3.8x10^4$, m = 3; d) $A_H = 0.2$, Ma = $3.9x10^4$, m = 4.

Interestingly, as shown in Figure 10, when the aspect ratio of the liquid bridge is decreased and, accordingly, the azimuthal wavenumber becomes higher, the pattern formed by the isolines of the temperature field evolves from the eccentric cold circular region visible in Figure 10a for m = 1 to a configuration displaying a regular polygonal structure (with number of sides equal to the wavenumber, as shown in Figures 10c and 10d, respectively), passing through a stage in which the shape of the inner cold region is elliptic (Figure 10b, m = 2).

For the sake of completeness (and to promote cross comparison with some of the dynamics which will be illustrated for the full zone in Sect. 4), however, we should expressly mention that the liquid bridge problem is known to gain complexity as the Marangoni number is further increased. In particular, when the Marangoni number *largely exceeds* the critical value, supercritical states with *coexisting fundamental modes* become possible (the resulting pattern in the cross section displays at the same time features relating to two or more different values of m, that is, the temperature distribution can give rise to complex polygonal irregular structures resulting from the superposition of different geometric shapes such as the fundamental ones shown in Figure 10). In order to understand this concept, it is sufficient to recall that the loss of symmetry generally implies the existence of a new solution that bifurcates from the initial state due to the selection and ensuing amplification of disturbances. Every time that the system undergoes a bifurcation, new disturbances are excited (a new mode m). If the characteristic number is increased many times, the bifurcations become faster (bifurcations sequence) and faster until the system becomes chaotic from both spatial and temporal points of view. The interested reader being referred to the studies by Frank and Schwabe (1997, 1999), Ueno et al. (2003ab), Shevtsova et al. (2003) for additional details.

3.2. Thermogravitational Flow

Though the amount of literature dedicated to the analysis of Marangoni flow in liquid bridges is really impressive, unfortunately only a handful of

results have been produced for what concerns the development of convective modes of *purely gravitational nature* in this specific configuration.

Obviously, as the interface is assumed to be adiabatic for the half zone, such modes can emerge only if heating is provided from below (top disk cold, bottom disk hot), the opposite situation (top disk hot, bottom disk cold) representing an intrinsically stable state (able to maintain initially quiescent and thermally diffusive conditions ad infinitum).

As another important distinguishing mark, buoyancy convection (Rayleigh-Bénard flow) can be excited only *if a given threshold is exceeded in terms of Rayleigh number* (unlike Marangoni flow for which *no threshold needs to be exceeded to produce axisymmetric fluid motion,* Lappa, 2009). A further difference is represented by the nature of the emerging thermogravitational flow, this being always steady and three-dimensional over a wide range of aspect ratios. In the following we refer to the linear stability analysis by Wanschura et al. (1996)

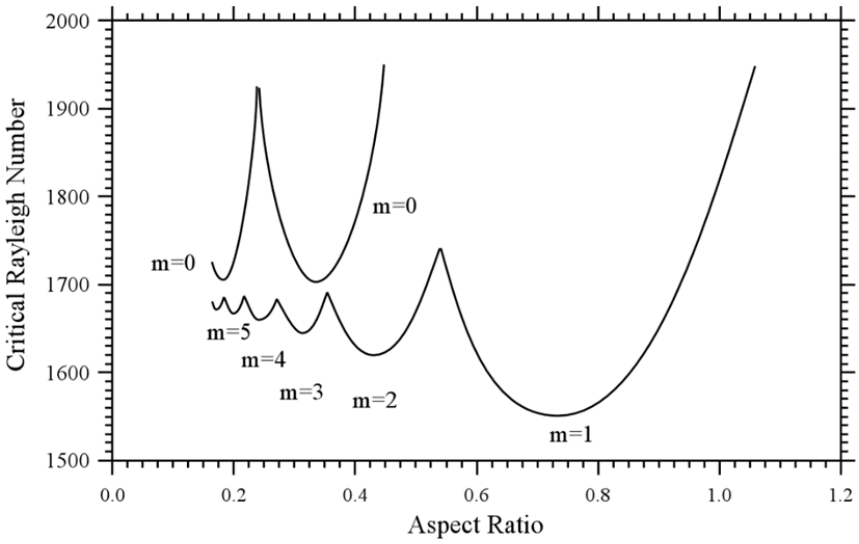

Figure 11. Stability limits for Rayleigh-Bénard convection in liquid bridges (Ra_{cr} based on the axial distance between the disks; courtesy of H. Kuhlmann).

These authors found a dependence of the critical wavenumber m on the liquid bridge aspect ratio such as that reported in Figure 11 (where it is also shown that the wavenumber m = 0, corresponding to axisymmetric flow, can enter the dynamics only for slightly larger values of Ra).

The origin of the convective disturbance pertaining to this specific mode of convection is much more intuitive if compared to the companion problem relating to the genesis of the waves in Marangoni flow. Yet, it can be illustrated in a relatively simple way by considering the impact of a localized hot disturbance on an initial quiescent fluid with unstable temperature stratification (i.e., a linear temperature distribution, see Figure 12).

Being lighter than the surrounding fluid, the parcel of fluids affected by the disturbance will obviously tend to rise, i.e., a rising current will be generated locally. As a result (due to continuity) other relatively warm fluid located underneath will be pulled up, thereby leading once again to a self-sustaining mechanism in which rising currents transporting hot fluid from the bottom towards the top cold boundary alternate in space with descending currents transporting relatively cold fluid in the opposite direction.

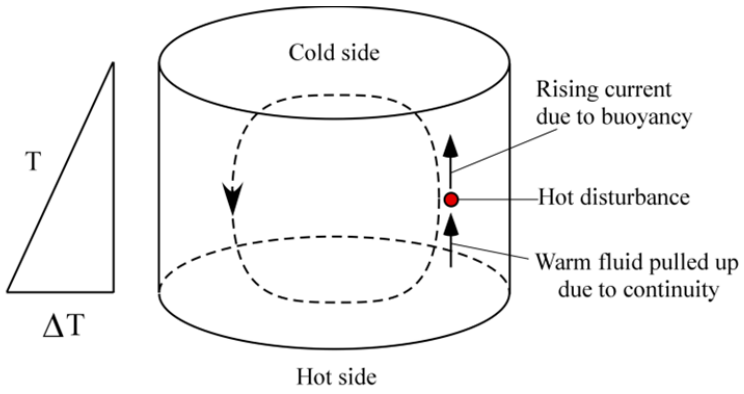

Figure 12. Amplification mechanism (sketch) leading to the emergence of Rayleigh-Bénard convection in a liquid bridge (heated from below, cooled from above and with adiabatic free surface).

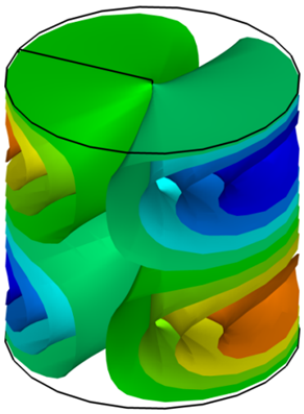

Figure 13. Isosurfaces of azimuthal velocity component for Rayleigh-Bénard convection in liquid bridge (A_H = 1, Pr = 28.1, Ra = $4x10^3$, steady state with m = 1, red and blue colors correspond to regions of positive and negative azimuthal velocity, respectively).

The notable difference relating to the origin of the 3D flow for Marangoni and RB convection also extends to the structure of related disturbances. Additional insights along these lines can directly be gathered from Figure 5.

While for Marangoni flow the isosurfaces of the azimuthal component of velocity look like curved "pillows" located in proximity to the free surface, for Rayleigh-Bénard convection they take the shape of 'bells' or multi-petal 'flowers' (with axes perpendicular to the axial direction and radial penetration depth equal to the radius of the liquid bridge, Figure 13).

Distinguishing marks, however, are not limited to the structure and stationary nature of the emerging 3D flow. What sets Rayleigh-Bénard (RB) convection apart, indeed, is its ability to produce *multiple states of convection*, that is, different solutions are allowed for the same (fixed) values of Ra and A_H. Such solutions exist in the space of parameters as independent attracting sets. However, the flow effectively emerging in a numerical simulation (or in the physical reality) essentially *depends on the specific initial conditions considered*. Using relevant language borrowed from the companion field relating to the analysis of non-linear systems,

these multiple solutions can generally be considered as coexisting "attractors" in the space of phases.

Accordingly, they can be identified or studied resorting to a specific strategy of analysis based on the variation of the related "basin of attraction" (that is the set of initial conditions that leads the trajectory of the system in the space of phases to meet a specific attractor).

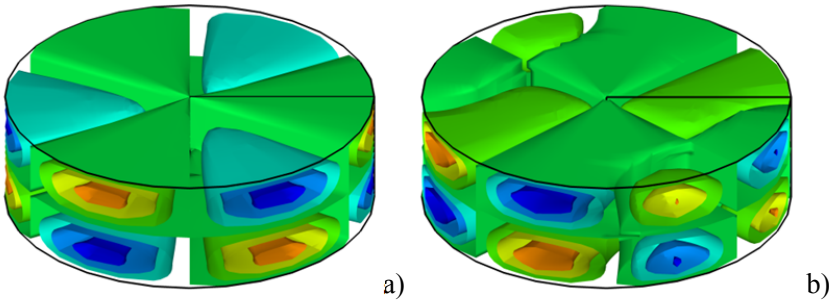

Figure 14. Isosurfaces of azimuthal velocity component for Rayleigh-Bénard convection in liquid bridge (A_H = 0.315, Pr = 28.1, Ra = $4x10^3$, red and blue colors correspond to regions of positive and negative azimuthal velocity, respectively) - Multiple steady solutions are possible: a) m = 3 (Mercedes pattern), b) four-roll state (initial conditions corresponding to 3D sinusoidal disturbances with arbitrary value of the azimuthal wavenumber added to a purely axisymmetric distribution of temperature, which increases linearly along the direction of gravity).

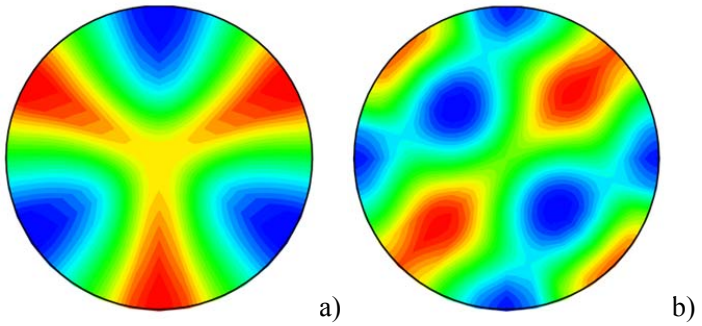

Figure 15. Temperature distribution in a section perpendicular to the liquid bridge axis for the same conditions shown in Figure 14 (red and blue colors correspond to regions of relatively hot and cold fluid, respectively).

For instance, Figures 14 and 15 show the different equilibrium states that can be attained by a liquid bridge heated from below (Pr = 28.1) with aspect ratio A_H = 0.315, for a fixed value of the Rayleigh number (Ra = 4000) when the initial conditions are changed. While, in one case (Figures 14a and 15a) a state with three localized peaks of negative and positive azimuthal velocity can be discerned (also known as "mercedes" structure by similarity with the logo of the well-known company, Borońska and Tuckerman, 2010a,b), in the other case (Figure 14b and 15b), the central symmetry of the pattern is no longer a recognizable feature; the flow in Figure 15b, indeed consists of four rolls all approximately aligned along the same direction (flow with dominant horizontal distribution of vorticity).

For the sake of completeness, we should mention expressly that these behaviors are not an exclusive prerogative of RB convection in liquid bridges as similar studies have been produced for the case of fluids encapsulated in cylindrical containers (no free liquid-gas lateral interface).

As an example, the interested reader may consider the experimental work by Hof et al. (1999), who could observe a multitude of steady stable patterns for the same final Rayleigh number Ra = 14200 in a cylinder with A = 0.25 and a fluid with Pr = 6.7. Such states were categorized as "rolls with hot fluid rising along the center", "rolls with cold fluid falling along the center", "spoke patterns with cold fluid falling along the spokes", "spoke patterns with hot fluid rising along the spokes" and "axisymmetric pattern with hot fluid rising in the center".

Similar results have also been obtained by means of numerical simulations. As an example, Borońska and Tuckerman, 2010a,b) re-examined the case originally addressed experimentally by Hof et al. (1999), with the intent to shed some additional light on the fascinating emergence of multiple solutions reported by those authors. In the experiments by Hof et al. (1999) a large number of convective patterns had been produced by increasing and decreasing the Rayleigh number in a variety of ways. Borońska and Tuckerman (2010a) explored the same parameter space using two different types of initial conditions (namely, quiescent fluid with a linear temperature distribution in the vertical

direction or fully developed flow). They initialized their numerical simulations with a slightly perturbed diffusive solution; such simulations provided different patterns, depending on Rayleigh number, which then were used as initial states *at other (smaller or larger) Rayleigh numbers*.

This study and other similar analyses have clarified that, unlike Marangoni flow in liquid bridges (which tend to favor 'axial vorticity'), RB convection emerging in cylindrical domains does not display necessarily the morphology of a toroidal roll (given its known tendency to produce parallel rolls, especially in relatively shallow containers as already shown in Figure 15b). Moreover, the liquid in the inner region can either be colder or warmer than that located more externally (for Marangoni flow in liquid bridges only the first condition is allowed).

Transition to time dependence is obviously possible also for RB convection (Lappa, 2009). For the case of convection in cylinders with aspect ratio of O(1), this transition generally occurs for relatively large values of the Rayleigh number (much higher that the value required for the onset of convection from the initial quiescent state). As illustrated by Boronska and Tuckermann (2006), in some circumstances these oscillatory modes can resemble those typical of Marangoni flow, i.e., traveling waves or standing waves.

3.3. Mixed Flow

While each of the convective effects considered in Sects. 3.1 and 3.2 on its own presents significant challenges to a full understanding of the physics controlling the behavior of the FZ, when combined they may even give rise to novel and/or unexplored phenomena. This has been clearly demonstrated by relevant studies produced over the years in which half zones supporting combined thermocapillary and thermogravitational effects (liquid bridge heated form below) have expressly been considered.

The main outcome of these studies (e.g., Wanschura et al., 1997 considered a liquid bridge with Pr = 4 and $A_H = 0.5$) is that, while in the absence of Marangoni effects there exist two equivalent convective

solutions potentially emerging from the thermally diffusive (quiescent) state, which consist of flow states with up or downflow at the center of the liquid bridge (corresponding to toroidal rolls with warm or relatively cold fluid in their center, respectively), for $B_d > 1$ the presence of weak surface-tension-driven effects can break this symmetry making the bifurcation 'imperfect'.

As a result, the emergence of a single toroidal vortex with sense of circulation supported by both buoyant and thermocapillary forces (surface fluid moving from the lower hot disk towards the upper cold one) is favored (generally known as *strong state* (a), see Figure 16a).

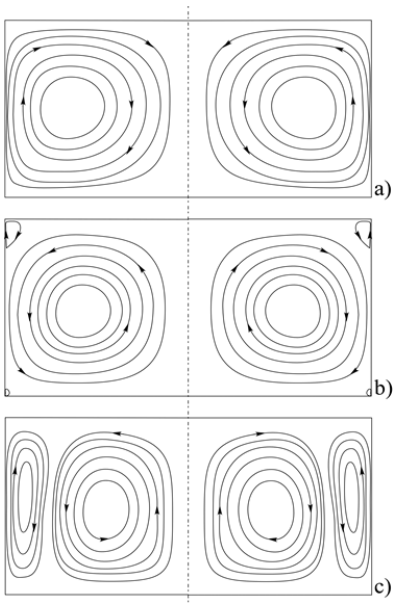

Figure 16. Multiple axisymmetric basic-flow solutions for hybrid Marangoni-buoyancy convection in half zones (for each sketch: heated and cooled disks on the bottom and on the top, respectively): (a) Strong state; (b) and (c) Weak states.

If the Rayleigh number is increased, however, other solutions become possible, namely the so-called weak states (b), and (c) shown in Figures 16b and 16c, respectively. For these states, buoyant and Marangoni effects oppose each other, and as a result, two alternate situations can be

established. In one case (weak state (b)), a strong internal toroidal vortex with fluid sinking along the free surface and rising in proximity to the axis is formed, while the surface-tension driven effects are confined to a small counter-rotating cell located in the corner between the cold (top) disk and the interface. Otherwise, two separate vortices can be maintained, with an external roll (featuring fluid rising along the interface), which takes an axially stretched shape and coexists with a counter-rotating internal one.

By studying the stability of these multiple axisymmetric (basic) states with respect to 3D disturbances, Wanschura et al. (1997) found the emerging three-dimensional flows to be essentially steady. Moreover, they even identified a range of Rayleigh numbers for which the axisymmetric convection is linearly re-stabilized and the two different axisymmetric states (a) and (b) can remain stable.

Similar analyses for the opposite situation in which Marangoni effects are dominant ($B_d < 1$) have shown that, regardless of whether the liquid bridge is heated from below or from above, the set of possible 3D modes is greatly reduced from the multiplicity allowed by pure Rayleigh-Bénard flow or mixed convection with $B_d > 1$ to the only two competing solutions already discussed in Sect. 3.1 for the case of pure Marangoni convection (i.e., *standing and traveling waves*).

Rotating and pulsating regimes have been observed both experimentally and numerically for mixed thermocapillary-thermogravitational flow in half zones over relatively wide regions of the space of parameters. Among other things, these studies have led to the conclusion that pulsating or rotating waveforms are generally selected depending on the considered initial conditions (in this regard they may still be regarded as "multiple solutions" associated to a specific basin of attraction like those of RB convection) and that the former are generally unstable as they tends to be replaced by traveling waves as time increases (Lappa et al., 2000).

The two fundamental situations considered over the years for $B_d < 1$ obviously differ with regard to the aiding or opposing roles of buoyancy and thermocapillarity. For the case in which the system is heated from below, the velocity along the free surface undergoes an increase in magnitude due to the combined effect of these two forces. In the opposite

conditions for which heating is applied from above, buoyancy and surface-tension-driven forces oppose each other at the free interface (in the absence of surface-tension effects the pattern would reduce to a linear thermally diffusive distribution of temperature in a motion-less liquid bridge).

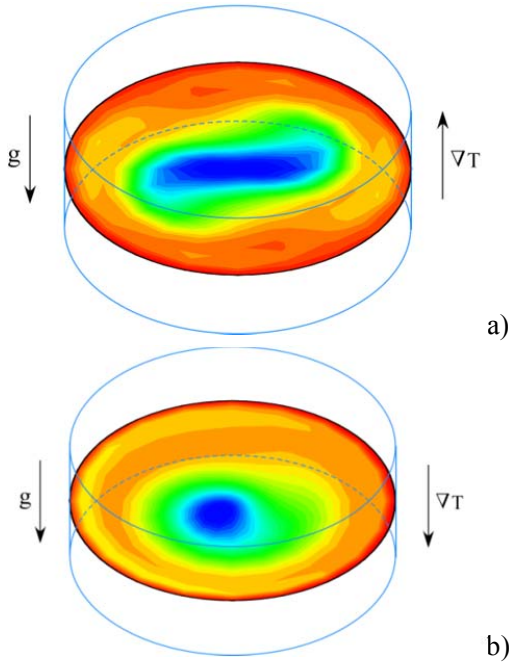

Figure 17. Snapshots of temperature distribution in a section perpendicular to the liquid bridge axis (A_H = 0.4, Pr = 30, liquid bridge in normal gravity conditions, red and blue colors correspond to regions of relatively hot and cold fluid, respectively): a) Ma = $3.6x10^4$, liquid heated from above, m = 2; b) Ma = $4.3x10^4$, liquid heated from below, m = 1.

In a rather counterintuitive way, mixed convection has been found to be much more stable when the heating from below is considered (Velten et al., 1991; Wanschura et al., 1997). Moreover, this condition can lead to significant changes in the emerging wavenumber with respect to the situation in which the liquid bridges is heated from above for the same set of parameters (A_H, Pr, Ra and Ma, Lappa et al., 2000, Figure 17).

Lappa et al. (2000) explained this trend on the basis of the physical mechanism responsible for the development of the instability, i.e., the sequence of stages of evolution shown in Figure 8. In particular, they ascribed the observed stabilization of Marangoni flow in liquid bridges heated from below to the expected weakened influence played by potential small surface temperature disturbances on the surface flow due to the increased strength of this flow induced by the coupling between Marangoni and buoyancy effects. An alternate point of view based on vorticity arguments was elaborated by Wanschura et al. (1997). According to these authors, the stabilization of the basic state of a half zone heated from below with respect to heating from above (or pure Marangoni flow) should be interpreted taking into account the incompatible nature of the axial vorticity associated with Marangoni flow and the horizontal vorticity favored by buoyancy convection (two mechanisms excluding each other thereby leading to stabilization of the basic state).

4. THE FULL ZONE

As illustrated in Sect. 3, we now are in a situation where the study of the half zone has reached a sort of maturity, in the sense that numerical and experimental techniques are in position to yield useful and relevant information concerning most of the questions we may ask on the problem.

The analysis of the full zone, however, is a considerably less developed area. This model does obviously introduce an additional level of complexity into the dynamics described so far (see, e.g., the experiments by Sakurai et al., 1998 and Kudo et al., 2014). As highlighted in Sect. 2.2, it carries another degree of freedom, namely the possibility for the flow to break the symmetry with respect to the equatorial plane. In the absence of gravity (pure Marangoni flow), this formally enables two different categories of 3D disturbances, i.e., modes which are *symmetric* (preserving the reflection symmetry) or *antisymmetric* (breaking the symmetry) with respect to $z = 0$ (Figure 1b).

Unfortunately, only a few theoretical studies addressing the bifurcation to 3D flow have been appearing in the literature for Pr > 1 (Chen, and Chieh, 1995; Lan, 2003; Bouizi et al., 2007; Motegi et al., 2017).

As an example, for pure Marangoni flow Bouizi et al. (2007) investigated the transition from the initial axisymmetric state to three-dimensional (3D) flow using a Chebyshev spectral numerical method over a relatively large range of Prandtl number values ($10^{-3} \leq Pr \leq 10^{2}$). It was shown that the main conclusions related to more than three decades of studies on the companion half-zone problem could qualitatively be applied to the full zone (the flow becoming unstable against oscillatory disturbances of hydrothermal nature, which manifest as "waves"). Antisymmetric modes and standing waves were found to be dominant in this study for the case of high-Pr fluids (e.g., Pr = 20 and Pr = 100).

Though, technically speaking, a classification of the disturbances based on the distinction in symmetric and antisymmetric modes would no longer be applicable to the full zone in the presence of gravity (as buoyancy effects clearly prevent the flow from retaining reflection symmetry with respect to the equatorial plane), Motegi et al. (2017) extended this nomenclature to this case loosely re-defining these two classes of disturbances as *modes for which the temperature disturbances occurring at a fixed azimuthal station above and below the equatorial plane have the same or opposite signs*.

In particular, considering conditions similar to those originally investigated by Wanschura et al. (2007) for the classical liquid bridge (half zone, see Sect. 3.3), Motegi et al. (2017) performed a linear stability analysis for a full zone with Pr = 4 and $A_F = 1$ and increasing values of the Rayleigh number. They found antisymmetric modes to be the most critical disturbances (like the case of microgravity conditions) for relatively small values of Ra (with buoyancy essentially leading to an appreciable increase in the value of the required critical Marangoni number). The antisymmetric modes, however, were observed to be taken over by symmetric disturbances as the most critical ones for a further increase in Ra (exceeding a given threshold). Moreover, this switch in the symmetry was found together with a remarkable change in the trend displayed by the

critical Marangoni number, starting to behave as a decreasing function of Ra beyond such a threshold. In this range of values of the Rayleigh number, most interestingly, these authors found the slope of the curve Ma(Ra) to become very steep, which they ascribed to *a transfer of the instability source from the toroidal roll in the upper half of the liquid bridge to the one in the lower half* induced by an increase in the buoyancy effect. According to their analysis, moreover, on further increasing Ra, symmetric hydrothermal disturbances are finally replaced by a non-oscillatory 3D mode similar to those previously found for the half-zone with dominant buoyancy.

Even though at this stage, on the basis of LSA results such as those yielded by Motegi et al. (2017), the reader might have already realized the increased level of complexity due to the interaction of Marangoni and buoyancy effects in the full zone, recent experiments have shown that reality might even be more complex.

As an example, Kudo et al. (2014) opened up a new perspective on the study of situations in which the Marangoni flow is dominant with the experimental discovery of a sort of chaotic state (for Pr = 28.1) in a region of the space of parameters where according to existing theories and earlier research studies for the half zone, mixed thermocapillary-thermogravitational convection should be laminar with a regular structure in space and a periodic behavior in time (single-frequency and single wavenumber flow).

Most interestingly, in such experiments, disturbances with different azimuthal wavenumbers m = 1, 2, and 3 were found *to coexist for slightly supercritical conditions* (i.e., as soon as the flow becomes unstable). Moreover, these modal structures were observed to behave in a relatively random (unpredictable) way, *switching irregularly from the typical dynamics of a standing wave to those of traveling waves and vice versa*.

These remarkable results have demonstrated that circumstances exist for which classical models might inherently be flawed.

Lappa (2016) addressed this apparent conundrum through solution of the Navier-Stokes equations (eqs. (1)-(3)) in their complete, time-dependent and non-linear form. For the same cases considered by Kudo et

al. (2014), notably, these numerical results have shown that this specific problem may yet been interpreted in the frame of models and theories about the existence of 'multiple solutions'.

As explained in Sects. 3.2 and 3.3, modes of convection, existing independently in the space of states, can manifest separately depending on the initial conditions. However, if the critical conditions for their onset are relatively close, they can also be excited at the same time thereby leading to *hybrid states*.

This concept, which is not straightforward as one would imagine, can be developed in a proper way starting from the description of the specific structure of the flow established in the generic meridian plane of the full zone (Figure 18).

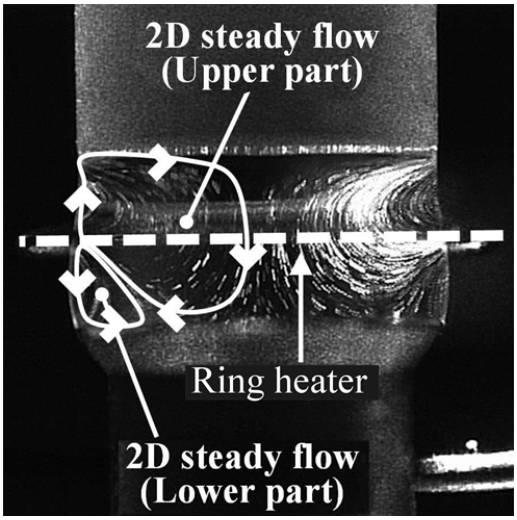

Figure 18. Typical structure of oscillatory Marangoni convection in the meridian plane of a full zone; Pr = 28.1, A_F = 0.68; courtesy of I. Ueno).

4.1. Spatial Flow Structure

As shown in Figure 18, in place of the single roll typically established in the half zone (Figure 3), two overlying toroidal rolls with different

strength and morphological properties represent the dominant convective systems in the full zone. The different flow structure and intensity are obviously related to the different interplay of the buoyancy and surface-tension-driven effects according to the considered region.

Roughly speaking, the upper half of the full zone can be seen as a liquid bridge heated from below, and vice versa for what concerns the lower half (akin to a half zone with heating from above). Notably, reversal of the dominant temperature gradient when crossing the equatorial plane (Figure 1b) implies that buoyancy can play the role of a force *aiding* surface Marangoni flow or *counteracting* it depending on the considered half (the reader being also referred to the similar arguments elaborated in Sect. 3.3). It is as a result of such effects that the upper roll is always stronger (due to concurrent Marangoni and buoyant effects) and extends to a large extent into the lower half (Kudo et al., 2014), thereby forcing the (weaker) bottom roll into a region of relatively small radial extension located in proximity to the liquid/gas interface (where it takes an axially stretched shape, Lappa, 2016).

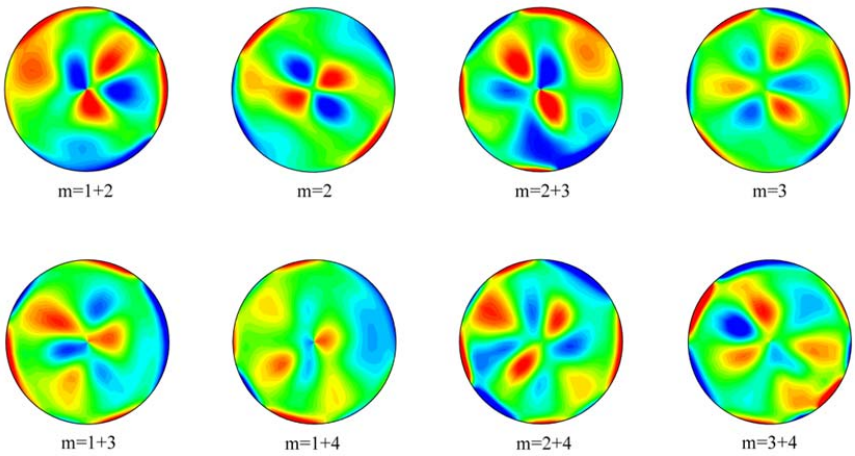

Figure 19. Snapshots of azimuthal velocity distribution at different times in cross-sections perpendicular to the full-zone axis (z = 1/2, upper half, $A_F = 0.63$, Pr = 28.1, Ma ≅ 2.3×10^4, Ra ≅ 4.2×10^3, red and blue colors correspond to regions of positive and negative azimuthal velocity, respectively).

In order to deal with such intricacies, Lappa (2016) examined the multicellular structures emerging due to the flow instability in selected cross sections (perpendicular to the z-axis) of the two opposing toroidal rolls located in the upper and lower halves of the full zone. For Pr = 28.1, A_F = 0.63, Ma ≅ 2.3x10^4, Ra ≅ 4.2x10^3, as an example, the 'multiplicity' of the involved azimuthal modes was found to be N = 4, with the azimuthal wavenumbers m = 1, 2, 3 and 4 manifesting at selected instants in isolated or combined form. Such instantaneous states are shown in Figures 19 and 20. These figures also provide interesting information on the relative amplitude of disturbances in the two opposing halves of the full zone. Indeed, by denoting with $f_{(down)m}(r,z,t)$ and $f_{(up)m}(r,z,t)$ the amplitude of the generic disturbance with azimuthal wavenumber *m* in the lower and upper roll, respectively, by cross-comparison of sections at z = 1/2 and z = -1/2, the reader will realize that for a given z > 0, the following inequality holds:

$$f_{(up)m}(r,z,t) \neq f_{(down)m}(r,-z,t), \quad \text{with} \quad \left|f_{(down)m}(r,-z,t)\right| \leq \left|f_{(up)m}(r,z,t)\right| \tag{16}$$

which in some circumstances and for some specific modes (compare Figures 19 and 20) even reduces to

$$f_{(down)m}(r,-z,t) \cong 0 \tag{17}$$

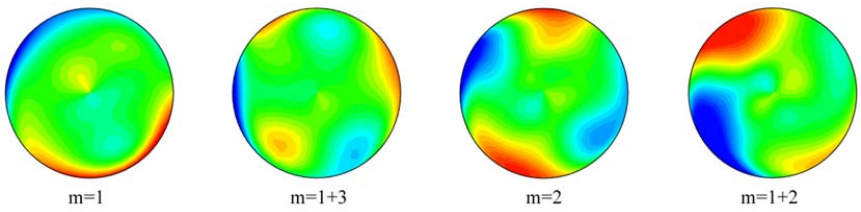

Figure 20. Snapshots of azimuthal velocity distribution at different times in cross-sections perpendicular to the full-zone axis (z = -1/2, lower half, A_F = 0.63, Pr = 28.1, Ma ≅ 2.3x10^4, Ra ≅ 4.2x10^3, red and blue colors correspond to regions of positive and negative azimuthal velocity, respectively).

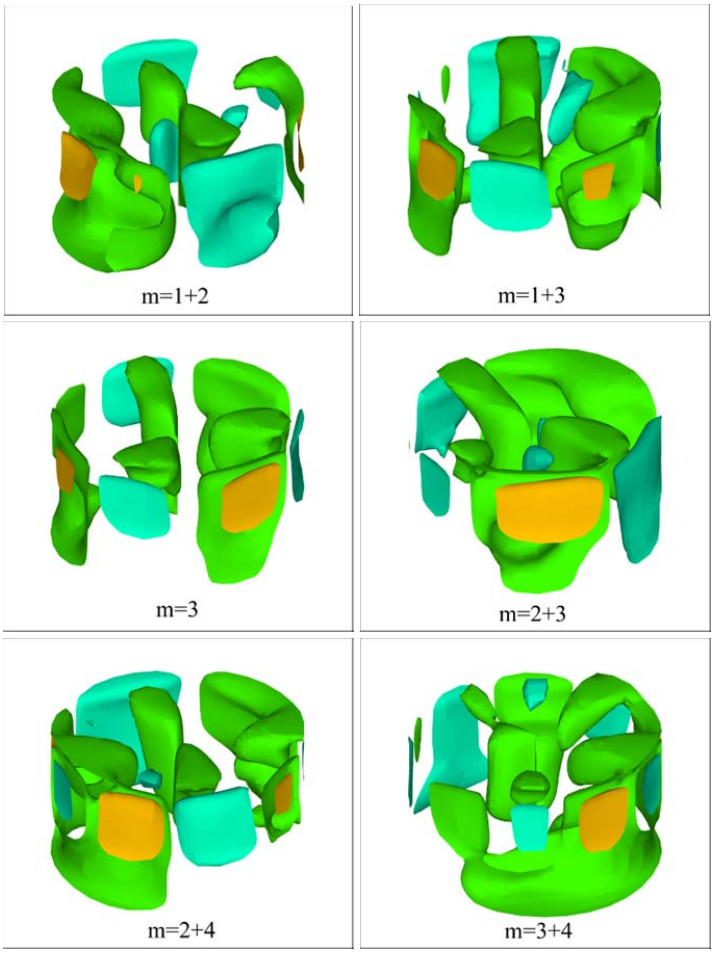

Figure 21. Isosurfaces of azimuthal velocity (snapshots) at different times ($A_F = 0.63$, $Pr = 28.1$, $Ma \cong 2.3x10^4$,$Ra \cong 4.2x10^3$). The isosurfaces correspond to three distinct values of the nondimensional azimuthal velocity (-7x10, 2x10, 1.1x10).

These results are particularly interesting for the insights they provide into the ability of coexisting toroidal rolls to increase the complexity in terms of disturbance evolution and related patterning behavior. In particular, while for the lower roll a limited number of modes is excited (disturbances with m = 1 and m = 2 in disjoint or combined form with some occasional manifestations of the m = 3 mode), a rich set of azimuthal

wavenumbers is allowed for the upper roll (m = 1,2,3,4 and related combinations or 'hybrid states' as explained before). The same conclusion can be drawn via careful analysis of the isosurfaces of the azimuthal velocity in space (Figure 21), where an abrupt change in the spatial structure of disturbances can be seen when the equatorial plane is crossed.

While perturbation 'nodes' are evident for $z > 0$ in the form of disjoint 'pillows' with different colors located along the circumferential direction, an almost patternless state is established for $z < 0$. As formalized by eq. (17), no disturbances with m = 3 and m = 4 can be identified under the equatorial plane (this equation being satisfied essentially in the large wavenumber part of the spectrum of disturbances).

4.2. Temporal Dynamics

Also in this case additional useful information on the considered phenomena can be obtained by resorting to an alternate point of view based on the analysis of temperature signals. Following the same approach illustrated in Sect. 3.1 for the half zone, the history of temperature recorded at fixed positions (by experimental or 'numerical' probes) distributed along the azimuthal direction (Figure 22) can help to discern the prevailing spatio-temporal behavior. Along these lines, Figure 23 obtained for the same case shown in Figures 19-21, is particularly meaningful.

Scattering of peaks for $z = 1/2$ (Figure 23a) as opposed to ordered accumulation of minima and maxima at certain temporal locations for $z = -1/2$ (Figure 23b), indeed, indicates that 'on average' the lower roll is characterized by a pulsating behavior, whereas the upper one supports disturbances propagating circumferentially (as already explained to a certain extent in Sect. 3.1, recognizable clustering of maxima and minima should be seen as the typical signature of spatially fixed disturbance nodes, whereas significant scattering of such extrema should be regarded as evidence for traveling waves).

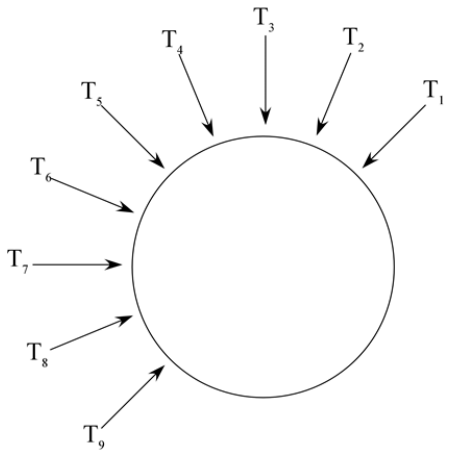

Figure 22. Sketch showing nine numerical thermocouples equally spaced along the azimuthal direction covering an angular extension of 180°.

Still following Lappa (2016), an explanation for this scenario can be elaborated in its simplest form resorting to a spatial perspective based on the simple realization that, as clarified in Sect. 4.1, the two overlying toroidal rolls have different properties.

Notably, if these rolls were completely independent, on the basis of past findings for the classical liquid bridge (Sect. 3), as a natural consequence of their different strength and geometrical properties they should undergo rather a different evolution. This argument might be used *as a first key argument to explain the observed differences in terms of prevailing disturbances in the two halves of the full zone and related spatio-temporal dynamics*.

Superimposed on these aspects, however, is the fact that the two rolls are not uncoupled, as *they can interact and exchange momentum and heat*.

In earlier studies focused on liquid metals (see, e.g., Lappa, 2003, 2004ab, 2005 for Marangoni flow in a full zone made of silicon melt), it was found that when a two-roll configuration is considered, the interaction between the two opposing toroidal convective systems can cause a significant decrease in the value of the critical Marangoni number with respect to the liquid-bridge case and make the supercritical state significantly more complex. A similar trend was also highlighted by

Gelfgat et al. (2000), who examined buoyancy convection in a cylindrical configuration relevant to the so-called vertical Bridgman crystal growth method. These authors identified several azimuthal modes which become critical at relatively close values of the Rayleigh number.

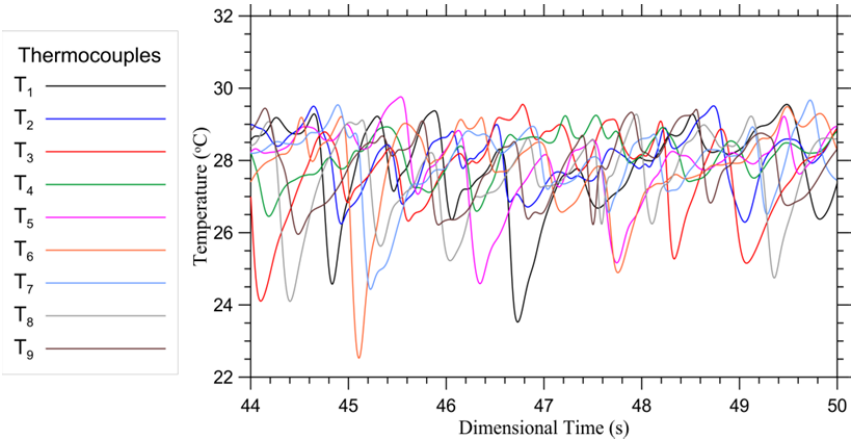

a)

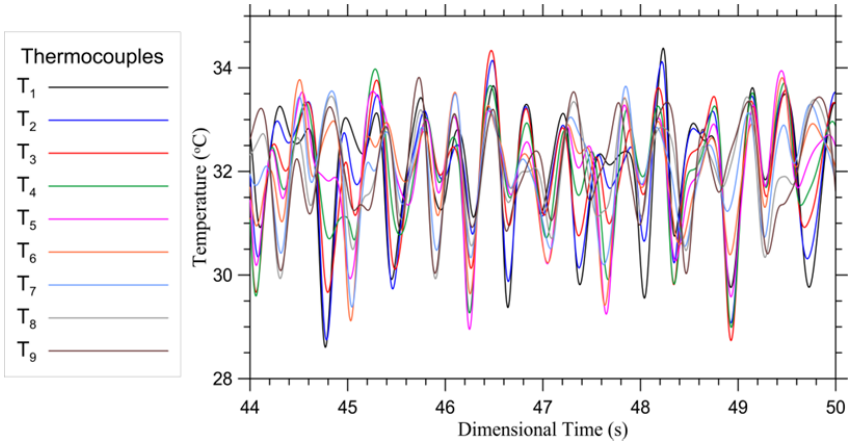

b)

Figure 23. Signals provided by the numerical probes shown in Figure 22 (A_F = 0.63, Ma ≅ 2.3x10^4, Ra ≅ 4.2x10^3): a) z = 1/2 (upper half), a continuous phase shift is allowed; b) z = -1/2 (lower half), only discrete values of phase shift can be seen.

These effects can still be invoked to justify the peculiar pattern-forming mechanism seen for the complete floating zone for Pr > 1. As explained before, two superposed toroidal rolls are embedded in the full zone, and it can be argued that their interaction can significantly expand the set of allowed instability modes (thereby lowering the critical threshold). Moreover, the multiplicity of solutions and their diversification according to the roll (upper or lower), can be justified according to the different geometrical properties of such convective systems and the effective interplay between gravitational and thermocapillary effects (which, in turn, depend on the relative position of the considered liquid region with respect to the equatorial plane).

The same arguments can also be used to explain the differences relating to the temporal behavior. According to Figure 23a, the prevailing flow in the upper larger roll can be interpreted as a combination of waves traveling with distinct azimuthal wavenumbers (m = 1,2,3,4) and different amplitudes, as witnessed by the variety of phase shifts displayed by the signals. By contrast, owing to the peculiar geometric configuration of the lower roll (axially stretched and with limited radial extension), the variety of modes is largely reduced (m = 1,2) and only two phase shifts are allowed, which indicates the coexistence of these disturbances results in standing-wave modes (waves that overlap with similar amplitude thereby leading to an essentially pulsating behavior).

As a final aspect deserving discussion, we limit ourselves to recalling that these arguments can also be used to shed some light on the apparently "intermittent" response of the system observed by Kudo et al. (2014). The random switching from the dominant rotating (pulsating) mode of convection to the pulsating (rotating) one can obviously be ascribed to the interference (non-linear interaction) among all such modes. Indeed, the related interconnected feedback loops can make the system extremely sensitive to the interaction between the upper and lower rolls. In turn, this effect can cause frequent changes in the *instantaneous* spatio-temporal mode of convection and allow intermediate (hybrid) situations in which the resulting scenario is apparently erratic (as confirmed by the numerical simulations by Lappa, 2016).

CONCLUSION

The production of oxide materials with the floating zone technique should be regarded as a relatively complex process if it is considered under the perspective relating to the convective modes which can potentially be excited in the melt.

This chapter has attempted to assemble a simple, physically intuitive and reasonably self-contained discussion of all the possible flow instabilities in liquid volumes with free cylindrical surface supporting both surface-tension driven and buoyancy convection.

These range from the classical axisymmetric mixed Marangoni-buoyancy convection and related supercritical three-dimensional regimes, which can be studied using a classical liquid bridge (half zone) held between differentially heated supporting disks, to the much more complex states enabled when heat is injected into the system through the lateral free surface (full zone).

The limited multiplicity of solutions known for pure or dominant Marangoni flow in half zones (just two alternate fundamental spatio-temporal modes of convection being allowed when the critical threshold for the onset of oscillatory convection is exceeded) is greatly expanded when pure buoyancy (Rayleigh-Bénard) convection is considered (liquid being uniformly heated from below). Remarkably, this is also a feature of mixed Marangoni-buoyancy convection in the full zone even though situations in which gravitational effects relatively weak with respect to thermocapillary ones are considered. Rather than being an intrinsic feature of the mixed convection, the multiplicity of modes allowed in this case results from the additional degree of freedom represented by symmetry rupture with respect to the equatorial plane and the coexistence of two toroidal rolls with different properties. Distinct azimuthal modes can become critical at the same time, thereby making the emerging flow apparently erratic in nature.

A general conclusion stemming from the present discussions is that the use of surrogate models of the real FZ allows more efficient exploration of wide regions of the space of parameters and, in this regard, the half zone

has proven instrumental in unraveling processes that are interwoven or overshadowed in a real floating zone. In the future, however, additional studies will be required to explore the behavior of the full zone, which still hides a not-fully-understood competition of complex and diverse physical mechanisms. It is expected that the fundamental information gained from these investigations will be crucial in our ambitious goal to elaborate a general theoretical framework for the FZ process and derive a generalized set of principles to predict its evolution in many circumstances.

ACKNOWLEDGMENTS

This work has been partially supported by UK Engineering and Physical Sciences Research Council (EPSRC grant EP/R043167/1) in the framework of the JEREMI project.

REFERENCES

Balbashov A.M. and Egorov S.K., (1981), "Apparatus for growth of single crystals of oxide compounds by floating zone melting with radiation heating", *J. Cryst. Growth*, 52: 498–504.

Balbashov A.M., Tsvetkova A.A., Chervonenkis A.Y., (1975), "Imperfections in crystals of yttrium-iron garnet grown from nonstoichiometric melts", *Neorg. Mater.*,11: 108–111.

Bazzi H., Nguyen C.T. and Galanis N., (1999), "Numerical simulation of oscillatory Marangoni convective flow inside a cylindrical liquid zone", *Int. J. Therm. Sci*., 38(10): 863-878.

Benz K.W., (1990), "Factors controlling crystal perfections during growth under microgravity", *Proceedings VIIth European Symposium on Materials and Fluid Sciences in Microgravity Oxford* (United Kingdom), 10/15 September , ESA SP 295: 59-61.

Boronska K. and Tuckermann L.S., (2006), "Standing and traveling waves in cylindrical Rayleigh–Bénard convection", *J. Fluid Mech.*, 559: 279-298.

Borońska K., Tuckerman L.S., (2010a), "Extreme multiplicity in cylindrical Rayleigh-Bénard convection: I. Time-dependence and oscillations", *Phys. Rev. E*, 81, 036320.

Borońska K., Tuckerman L.S., (2010b), "Extreme multiplicity in small aspect ratio Rayleigh-Bénard convection: II. Bifurcation diagram and symmetry classification", *Phys. Rev. E*, 81, 036321.

Bouizi O., Delcarte C., Kasperski G., (2007), "Stability study of the floating zone with respect to the Prandtl number value", *Phys. Fluids* 19, 114102.

Chen C.J. and Chieh H., (1995), "Measurement of the float-zone interface shape for lithium niobate", *J. Cryst. Growth*, 149: 87–95.

Chen G., Lizee A., Roux B., (1997), "Bifurcation analysis of the thermocapillary convection in cylindrical liquid bridges", *J. Cryst. Growth*, 180: 238-247.

Chun C.H. and Siekmann J., (1995), "Higher modes and their instabilities of the oscillating Marangoni convection in a large cylindrical liquid column", *Proceedings of the Norderney Symposium on Scientific Results of the German Spacelab Mission D2,* Editors P.R. Sahm, M.H. Keller, B. Schiewe, 235-241.

Chun C.H., (1980), "Experiments on steady and oscillatory temperature distribution in a floating zone due to the Marangoni convection", *Acta Astronautica*, 7: 479-488.

Cröll A., Kaiser Th., Schweizer M., Danilewsky A.N., Lauer S., Tegetmeier A., Benz K.W., (1998), "Floating-zone and floating-solution-zone growth of GaSb under microgravity", *J. Cryst. Growth*, 191: 365-376.

Dabkowska H.A. and Dabkowski A.B., (2010), "Crystal Growth of Oxides by Optical Floating Zone Technique", in Springer *Handbook of Crystal Growth* 367 (2010), pp. 367-391.

Dabkowska H.A. and Gaulin B.D., (2003), *"Crystal Growth of Technologically Important Electronic Materials",* ed. by K. Byrappa, T. Ochachi, M. Klapper, R. Fornari (Allied Publishers PVT, New Delhi 2003) pp. 341–354.

Frank S. and Schwabe D., (1997), "Temporal and spatial elements of thermocapillary convection in floating zones", *Exp. Fluids*, 23: 234-251.

Frank S. and Schwabe D., (1999), "Experiments on the transition to chaotic thermocapillary flow in floating zones under microgravity", *Adv. Space Res.*, 24(10): 1391-1396.

Gelfgat A.Yu., Bar-Yoseph P.Z., Solan A., (2000), "Axisymmetry breaking instabilities of Natural convection in a vertical Bridgman growth configuration", *J. Cryst. Growth*, 220: 316-325.

Higuchi M. and Kodaira K., (1992), "Effect of ZrO_2 addition on FZ growth of rutile single crystals", *J. Cryst. Growth*, 123: 495–499.

Hof B., Lucas, G.J. and Mullin T., (1999), "Flow state multiplicity in convection", *Phys. Fluids*, 11: 2815-2817.

Hurle D.T.J. (Ed.), (1994), *Handbook of crystal growth,* North-Holland, Amsterdam, 1994.

Kimura S. and Kitamura K., (1992), "Floating zone crystal growth and phase equilibria: A review", *J. Am. Ceram. Soc.*, 75(6): 1140–1146.

Kudo M., Ueno I. and Kawamura H., (2014), "Transition of thermocapillary convection in a full-zone liquid bridge", *Transactions of the JSME* (in Japanese), 80(812) (15 pages), [DOI: 10.1299/ transjsme.2014tep0095].

Kuhlmann H.C. and Rath H.J., (1993a), "Hydrodynamic instabilities in cylindrical thermocapillary liquid bridges", *J. Fluid Mech*., 247: 247-274.

Kuhlmann H.C. and Rath H.J., (1993b), "On the interpretation of phase measurements of oscillatory thermocapillary convection in liquid bridges", *Phys. Fluids* A 5 (9): 2117-2120.

Kuhlmann H.C., (1995), "Some scaling aspects of thermocapillary flows", *Microgravity Q.*, 5: 29-34.

Lan C.W., (2003), "Three-dimensional simulation of floating-zone crystal growth of oxide crystals", *J. Cryst. Growth*, 247: 597–612.

Lappa M., (1995), *"Marangoni flow instabilities in liquid bridges in microgravity",* MSc Thesis, University of Naples.

Lappa M., (2003), "Three-dimensional numerical simulation of Marangoni flow instabilities in floating zones laterally heated by an equatorial ring", *Phys. Fluids*, 15(3): 776-789.

Lappa M., (2004a), "Combined effect of volume and gravity on the three-dimensional flow instability in non-cylindrical floating zones heated by an equatorial ring", *Phys. Fluids*, 16(2): 331-343.

Lappa M., (2004b), "Floating zones heated around the equatorial plane: models and simulations", *Microgravity Sci. Tech.*, XV/3: 36-51.

Lappa M., (2005), "Analysis of flow instabilities in convex and concave floating zones heated by an equatorial ring under microgravity conditions", *Computers & Fluids*, 34(6): 743-770.

Lappa M., (2007), "On the stability and prominent features of Marangoni flow in classical models of the Floating Zone Technique in normal and microgravity conditions", Chapter 5 (pp. 83-128) in *Studies on Flow Instabilities in Bulk Crystal Growth*, Editor Alexander Gelfgat, ISBN-10: 81-7895-277-7, ISBN-13: 978-8178952772, 2007, Transworld Research Network (Research Signpost).

Lappa M., (2009), *Thermal Convection: Patterns, Evolution and Stability,* John Wiley & Sons, Ltd (2009, Chichester, England).

Lappa M., (2012), *Rotating Thermal Flows in Natural and Industrial Processes,* John Wiley & Sons, Ltd (2012, Chichester, England).

Lappa M., (2016), "On the onset of multi-wave patterns in laterally heated floating zones for slightly supercritical conditions", *Phys. Fluids*, 28(12), 124105 (22 pages).

Lappa M. and Ferialdi H., (2019), *"Oscillatory and Turbulent Flows of Liquid Metals in Differentially Heated Systems with Horizontal and Non-horizontal Walls"*, this book.

Lappa M., Savino R. and Monti R., (2000), "Influence of buoyancy forces on Marangoni flow instabilities in liquid bridges", *Int. J. Num. Meth. Heat Fluid Flow*, 10 (7): 721-749.

Lappa M., Savino R. and Monti R., (2001), "Three-dimensional numerical simulation of Marangoni instabilities in liquid bridges: influence of geometrical aspect ratio", *Int. J. Num. Meth. Fluids*, 36 (1): 53-90.

Leypoldt J., Kuhlmann H.C., Rath H.J., (2000), "Three-dimensional numerical simulation of thermocapillary flows in cylindrical liquid bridges", *J. Fluid Mech*, 414: 285-314.

Melnikov D.E., Shevtsova V.M. and Legros J.C., (2005), "Route to aperiodicity followed by high Prandtl-number liquid bridge. 1-g case", *Acta Astronautica*, 56(6): 601-611.

Moest B., Glebovsky V.G., Brongersma H.H., Bergmans R.H., Denier van der Gon A.W., Semenov V.N., (1998), "Study of Pd single crystals grown by crucibleless zone melting", *J. Cryst. Growth*, 192(3-4): 410–416.

Monti R., (1987), "On the onset of the oscillatory regimes in Marangoni flows", *Acta Astronautica*, 15: 557-560.

Monti R., Albanese C., Carotenuto C., Castagnolo D., Ceglia E, (1995), "First Results from Onset Experiment during Spacelab Mission D-2", *Proceedings of the Norderney Symposium on Scientific Results of the German Spacelab Mission D2,* Editors P.R. Sahm, M.H. Keller, B. Schiewe, 247-258.

Monti R., Savino R., Lappa M. and Fortezza R., (1998), "Scientific and technological aspects of a sounding rocket experiment on oscillatory Marangoni flow", *Space Forum* (ISSN 1024-803X), 2(4): 293-318.

Motegi K., Kudo M., and Ueno I., (2017), "Linear stability of buoyant thermocapillary convection for a high-Prandtl number fluid in a laterally heated liquid bridge", *Phys. Fluids*, 29, 044106.

Muller G., (1988), *"Convection and inhomogeneities in crystal growth from the melt",* in H. C: Freyhard (Ed.), Crystals: Growth, Properties and Applications 12, Springer, Berlin.

Neitzel G.P., Chang K.T., Jancowski D.F., Mittelmann H.D., (1992), "Linear stability of thermocapillary convection in a model of the float-zone crystal-growth process", *Phys. Fluids* A 5: 108-114.

Ohta H. and Hosono H., (2004), "Transparent oxide optoelectronics", in *Materials Today,* ISSN:1369 7021, Elsevier Ltd 2004, pp. 42-51.

Otani S., Tanaka T., Ishizawa Y., (1988), "Control of heat flow to feed rod in floating zone system", *J. Cryst. Growth*, 87: 175–179.

Preisser F., Schwabe D., Scharmann A., (1983), "Steady and oscillatory thermocapillary convection il liquid columns with free cylindrical surface", *J. Fluid Mech*., 126: 545-567.

Revcolevschi A. and Jegoudez J., (1997), "Growth of large high-Tc single crystals by the floating zone method: A review", *Progr. Mater. Sci.*, 42: 321–339.

Rivas D. and Vazquez–Espi C., (2001), "An analysis of lamp irradiation in ellipsoidal mirror furnaces", *J. Cryst. Growth*, 223: 433–445.

Sakurai M., Tamura A., Kinoshita A. and Hirata A., (1998), "Marangoni convection in a liquid bridge that is heated by a ring heater in a full zone model", *Journal of The Japan Society of Microgravity Application*, 15: 419-424.

Saurat M. and Revcolevschi A., (1971), "Preparation by the floating zone method of refractory oxide monocrystals, in particular gallium oxide, and study of some of their properties", *Revue Internationale des Haute Temperatures et des Refractaires* 8: 291-304.

Savino R., Monti R., Lappa M., Castagnolo D. and Fortezza R., (2001), "Preliminary results of the sounding rocket experiment on oscillatory Marangoni flows in liquid bridge" (PULSAR II Experiment), *52th Congress of the International Astronautical Federation,* Tolosa, Oct. 1-5 2001, IAF-01-J.3.03.

Schwabe D. , Preisser F., Scharmann A., (1982), "Verification of the oscillatory state of thermocapillary convection in a floating zone under low gravity", *Acta Astronautica* 9 (4): 265-273.

Schwabe D. and Scharmann A., (1984), "Microgravity experiments on the transition from laminar to oscillatory thermocapillary convection in floating zones", *Adv. Space Res*., 4(5): 43-47.

Schwabe D., (2002), "Standing waves of oscillatory thermocapillary convection in floating zones under microgravity observed in the experiment maus G141", *Adv. Space Res*., 29(4): 651-660.

Schwabe D., (2005), "Hydrothermal waves in a liquid bridge with aspect ratio near the Rayleigh limit under microgravity", *Phys Fluids*, 17, 112104 *(8 pages).*

Shevtsova V., Mialdun A., Kawamura H., Ueno I., Nishino K. and Lappa M., (2011), "Onset of Hydrothermal Instability in Liquid Bridge. Experimental Benchmark", *Fluid Dyn. Mater. Process*, 7(1): 1-28.

Shevtsova V.M., Melnikov D.E. and Legros J.C., (2003), "Multistability of oscillatory thermocapillary convection in a liquid bridge", *Phys. Rev. E*, 68 (6), 066311 (14 pages).

Shevtsova V.M., Melnikov D.E., Legros J.C., (2001), "Three-dimensional simulations of hydrodynamical instability in liquid bridges: influence of temperature-dependent viscosity", *Phys Fluids,* 13: 2851-2865.

Shindo I., (1980), "Determination of the phase diagram by the slow cooling float zone method: The system MgO-TiO_2" , *J. Cryst. Growth*, 50: 839–851.

Shindo I., Ii N., Kitamura K., Kimura S., (1979), "Single crystal growth of substituted yttrium iron garnets $Y_3Fe_{5-x}(Ga,Al)_xO_{12}$ by the floating zone method", *J. Cryst. Growth*, 46: 307–313.

Stadler A., (2012), "Transparent Conducting Oxides - An Up-To-Date Overview", *Materials*, 5: 661-683.

Tang Z.M., Hu W.R., Chen G., Roux B., (1997), "Numerical simulation of 3D thermocapillary oscillatory convection", *Microgravity Q.*, 7(2): 37-42.

Ueno I., Tanaka S. and Kawamura H., (2003a), "Oscillatory and chaotic thermocapillary convection in a half-zone liquid bridge", *Phys. Fluids*, 15(2): 408-416.

Ueno I., Tanaka S. and Kawamura H., (2003b), "Various flow patterns in thermocapillary convection in half-zone liquid bridge of high Prandtl number fluid", *Adv. Space Res*., 32(2): 143-148.

Velten R., Schwabe D., Scharmann A., (1991), "The periodic instability of thermocapillary convection in cylindrical liquid bridges", *Phys. Fluids* A 3: 267-279.

Villora E.G., Shimamura K., Yoshikawa Y., Aoki K., Ichinose N., (2004), "Large-size β-Ga_2O_3 single crystals and wafers", *J. Cryst. Growth*, 270: 420–426.

Wanschura M., Kuhlmann H.C., Rath H.J., (1996), "Three-dimensional instability of axisymmetric buoyant convection in cylinders heated from below", *J. Fluid Mech*., 326: 399-415.

Wanschura M., Kuhlmann H.C., Rath H.J., (1997), "Linear stability of two-dimensional combined buoyant-thermocapillary flow in cylindrical liquid bridges", *Phys. Rev. E*, 55 (6): 7036-7042.

Wanschura M., Shevtsova V., Kuhlmann H.C., Rath H.J., (1995), "Convective instability mechanism in thermocapillary liquid bridges", *Phys. Fluids*, 5: 912-925.

Watauchi S., Razzaque Sarker Md. A., Nagao M., Tanaka I., Watanabe T., Shindo I., (2012), "Crystal growth of rutile by tilting-mirror-type floating zone method", *J. Cryst. Growth*, 360(1): 105-110.

Yasuhiro S., Sato T., Imaishi N., (1997), "Three dimensional oscillatory Marangoni flow in a half zone of Pr = 1.02 fluid", *Microgravity Sci. Technol*., X/3: 144-153.

Yasuhiro S., Imaishi N., Kuhlmann H.C., Yoda S., (1999), "Numerical simulation of three dimensional oscillatory thermocapillary flow in a half zone of Pr = 1 fluid", *Adv. Space Res*., 24: 1385-1390.

Zeng Z., Mizuseki H., Chen J., Ichinoseki K. and Kawazoe Y., (2004), "Oscillatory Thermocapillary Convection in Liquid Bridge under Microgravity", *Materials Transactions*, 45 (5): 1522-1527.

Zeng Z., Mizuseki H., Higashino K., Kawazoe Y., (1999a), "Direct numerical simulation of oscillatory Marangoni convection in cylindrical liquid bridges", *J. Cryst. Growth*, 204: 395-404.

Zeng Z., Mizuseki H., Ichinoseki K., Higashino K., Kawazoe Y., (1999b), "Marangoni Convection in Half-Zone liquid Bridge", *Materials Transactions*, JIM, 40(11): 1331-1336.

RR